# Stability of a biomembrane tube covered with proteins

Mathijs Janssen,[1,2,3,*] Susanne Liese,[4,†] Sami C. Al-Izzi,[1,‡] and Andreas Carlson[1,§]

[1]*Department of Mathematics, Faculty of Mathematics and Natural Sciences, University of Oslo, 0315 Oslo, Norway*
[2]*Centre for Cancer Cell Reprogramming, Faculty of Medicine, University of Oslo, Montebello, N-0379 Oslo, Norway*
[3]*Norwegian University of Life Sciences, Faculty of Science and Technology, 1433 Ås, Norway*
[4]*Institute of Physics, University of Augsburg, 86159 Augsburg, Germany*

(Received 28 September 2022; accepted 29 February 2024; published 3 April 2024)

Membrane tubes are essential structural features in cells that facilitate biomaterial transport and inter- and intracellular signaling. The shape of these tubes can be regulated by the proteins that surround and adhere to them. We study the stability of a biomembrane tube coated with proteins by combining linear stability analysis, out-of-equilibrium hydrodynamic calculations, and numerical solutions of a Helfrich-like membrane model. Our analysis demonstrates that both long- and short-wavelength perturbations can destabilize the tubes. Numerical simulations confirm the derived linear stability criteria and yield the nonlinearly perturbed vesicle shapes. Our study highlights the interplay between membrane shape and protein density, where the shape instability concurs with a redistribution of proteins into a banded pattern.

DOI: 10.1103/PhysRevE.109.044403

## I. INTRODUCTION

Ubiquitous and essential in biology, phospholipid membranes are self-assembled fluid bilayers of nanometer thickness that compartmentalize biomaterial and form the boundaries of organelles. These bilayer membranes behave tangentially as incompressible fluids in which particles such as proteins can freely diffuse but display elastic behavior on deformations in the normal direction. This combination of resisting bend while allowing for tangential flow is a property that leads to a wealth of interesting vesicle shapes on mesoscopic length scales [1]. Of particular interest to biologists and physicists are cylindrical vesicles or membrane tubes, which can be formed from the action of a localized force on a flat membrane. In the simplest case, their radius $R = \sqrt{\kappa/2\sigma}$ is set by a balance between the bending rigidity of the membrane, $\kappa$, and surface tension, $\sigma$ [2,3]. In cells, membrane tubes can be formed by the action of molecular motors [4] and are part of organelles that enable biomaterial exchange and intra- and extracellular communication [5,6]. While some membrane tubes arise transiently [7,8], others can be long-lived parts of organelles, such as in the peripheral endoplasmic reticulum. In either case, the interaction between the tube membrane and the surrounding proteins is crucial for its emergence, shaping, and stability [9].

As the bilayer is thin compared to the size of the vesicles, it is often modelled as a two-dimensional (2D) surface. The classical model for this surface is due to Helfrich, who expressed the free energy of a membrane in terms of its mean and Gaussian curvatures, the lowest-order expansion of a general bending geometric free energy in terms of its principle curvatures [10–13]. Zhong-Can and Helfrich showed that a membrane tube of radius $R$ becomes unstable if the membrane's induced curvature is smaller than $-1/(2R)$ [14,15]. This instability, reminiscent of the Rayleigh-Plateau instability of liquid jets, causes membrane tubes to "pearl" for membrane surface tensions $\sigma$ exceeding $\sigma > 3\kappa/2R^2$ [16–20].

There is extensive literature on how particles—nearby, attached, or inserted into a membrane—affect membrane shape. Examples include the effects of different types of lipids [21–30], polymers [31–35], nanoparticles [36–40], phospholipid-surfactant mixtures [41], protein pumps [20,42], protein filaments [43,44], adsorbed BAR proteins [45–50], intercalated curvature-inducing proteins [51–53], and crowds of sterically repelling proteins [54–58] (see also reviews in Refs. [59–61]). Generally speaking, the total free energy of such systems contains, besides the Helfrich free energy, the free energy of the particles and a term accounting for the interaction of the membrane with the particles. Expressions for the free energy of the particles often contain terms penalizing phase boundaries [22,41,45,51,62] and terms accounting for interactions between the particles and for entropy, either through a Flory-Huggins theory for a mixture of occupied and unoccupied sites [21,27,33,41,45] or a Ginzburg-Landau expansion thereof [22,51,63]. To describe the interaction of particles with a vesicle, most authors [21,22,33,35,41,45,48,51–53,62,64,65] considered a linear coupling $\propto \Lambda H\phi$ of the mean curvature $H$ to the areal particle density $\phi$ with a coupling parameter $\Lambda$; this is the first term in an expansion of the free energy in $\phi$ and $H$ permitted by symmetry. Leibler showed that such interaction between proteins and a flat membrane sheet changes its effective bending rigidity to $\kappa - \Lambda^2/a$, with $a$ setting the strength of mutual

*mathijs.a.janssen@nmbu.no
†susanne.liese@physik.uni-augsburg.de
‡samiali@uio.no
§acarlson@math.uio.no

 

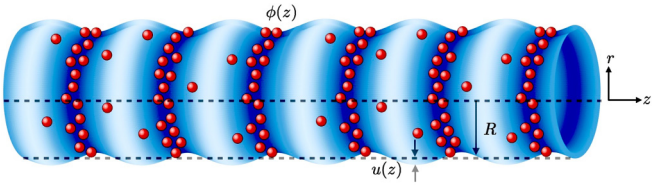


FIG. 1. Schematic of a lipid bilayer tube with attached particles. The membrane tube can undergo an instability from a homogeneously coated cylinder of radius $R$ towards an undulating shape $r(z) = R + u(z)$ and varying areal particle density $\phi(z)$. This sketch corresponds to a case for which the protein-membrane interaction parameter $\Lambda > 0$. For $\Lambda < 0$, bands of large protein concentration are at the crests instead.

protein interactions [51]. Consequently, the sheet becomes unstable to ruffles for $\kappa < \Lambda^2/a$.

Experiments have shown that membrane tubes with anchored polymers undergo a pearling instability similar to the tension-induced pearling of uncoated membrane tubes [33,58]. The experimentally observed tube shapes were interpreted through a theoretical model based on a free-energy description of surfaces of constant mean curvature. However, a comprehensive analysis of the stability of membrane tubes covered with rotationally symmetric (e.g., conical) protein inclusion is still lacking. As tubules are the simplest geometric shape with extrinsic curvature, they provide an ideal test bed for the coupling between extrinsic membrane curvature and redistributing proteins on that membrane.

This paper uses thermodynamic and hydrodynamic approaches to describe the mechanics of membrane tubes with curvature-coupled proteins. We show that in contrast to the flat membrane case, the extrinsic curvature of the tube radius gives rise to a bimodal growth rate for sufficiently high values of protein curvature coupling. When hydrodynamic effects are accounted for, the shorter wavelength instability dominates with a growth timescale set by the membrane viscosity. Finally, we present solutions to the nonlinear shape equation consisting of separate dense and dilute regions of constant mean curvature with an effective line tension between the different regions. Our results give a range of predictions for the shape of protein-covered membrane tubes that have potential relevance to a broad range of cellular processes, such as ER-Golgi transport [7,8] and mitochondrial fission [66,67].

## II. EQUILIBRIUM THEORY

### A. Setup

We consider a membrane tube and particles interacting with the membrane and among themselves (see Fig. 1). Without loss of generality, we refer to these particles as proteins. We partition the total free energy $F = F_H + F_\phi$ into a bare membrane term, given by the Helfrich free energy,

$$F_H = \int dA(2\kappa H^2 + \sigma) - P\int dV, \tag{1}$$

and a contribution $F_\phi$ due to the proteins. In Eq. (1), $H$ is the mean curvature, where our sign convention is such that a cylinder of radius $R$ has $H = -1/(2R)$. We use the typical value $\kappa = 20k_BT$ [68] for the bending rigidity, where $k_BT$ is the thermal energy. As $\kappa$ is positive, the first term in Eq. (1) penalizes membrane bending and thus resists membrane pearling. Moreover, $P$ is the pressure difference between the fluids inside and outside the tube, and $\sigma$ is the surface tension that acts along the entire membrane, typically around $\sigma = 2 \times 10^{-5}\,\mathrm{N\,m^{-1}}$ [12,69]. We omit a Gaussian bending term from Eq. (1), which is topologically invariant if we assume the saddle-splay modulus is a constant [12,70]. In principle, this term could contribute to the energy if the saddle-splay modulus depended on the protein concentration.

In addition to $F_H$, we consider the following Ginzburg-Landau free energy for proteins and their interaction with the membrane:

$$F_\phi = \int dA\left(-\Lambda\phi H - \mu\phi + \frac{a}{2}\phi^2 + \frac{b}{2}|\nabla\phi|^2\right). \tag{2}$$

Here $\phi$ is the areal protein density, satisfying $\phi \geqslant 0$, and $\nabla$ is the surface gradient operator, $\mu$ is the energy (per unit area) associated with protein binding to the membrane, $a$ sets the protein-protein repulsive interactions, and $b$ sets the cost of phase separation. We consider $a, b > 0$, such that the last two terms in Eq. (2) favor a vesicle with a homogeneous protein coat; $-\Lambda\phi H$, with $\Lambda$ setting the strength of protein-membrane interactions, is the only term in Eqs. (1) and (2) that can drive the system away from the straight-tube-homogeneous-coat energy minima. We consider both $\Lambda < 0$ and $\Lambda > 0$. For $\Lambda > 0$, the first term in Eq. (2) may lead to undulating ("pearling") tube shapes that minimize the free energy by recruiting and clustering proteins (large $\phi$) to regions where $H > 0$ (the troughs) while depleting them (small $\phi$) from regions where $H < 0$ (the crests). Conversely, $\Lambda < 0$ may lead to undulations with increased protein density at the undulating tube's crests. Experimental data for the values of $a$, $b$, and $\Lambda$ are scarce, but we make order-of-magnitude estimates for them in Appendix A. Appendix B reviews prior work on the stability of flat protein-covered membranes that used free-energy formulations similar to Eqs. (1) and (2).

### B. Stability analysis (cylindrical tube)

From hereon, we describe the membrane shape using cylindrical coordinates $(r, \theta, z)$ and consider a rotationally symmetric tube [20], such that all variables are $\theta$ independent. We first study the stability of a membrane tube of length $L$ and fixed radius $r(z) = r$ with a homogeneous coat of proteins at density $\phi(z) = \phi$. In this case, Eqs. (1) and (2) simplify to

$$\frac{F}{\pi L} = \frac{\kappa}{r} + 2r\sigma - Pr^2 + \Lambda\phi - 2r\mu\phi + a\phi^2 r. \tag{3}$$

For the free energy $F$ to be in a local minimum at a given $r = R$ and $\phi = \Phi$, three conditions must be met. First, minimizing Eq. (3) with respect to the protein density $[(\partial F/\partial\phi)_{R,\Phi} = 0]$ yields

$$\mu = a\Phi + \frac{\Lambda}{2R}, \tag{4}$$

which means that, unlike a membrane sheet [51], a membrane tube has a finite protein density $\Phi \neq 0$ if $\mu = 0$. Second, minimizing Eq. (3) with respect to the vesicle radius

$[(\partial F/\partial r)_{R,\Phi} = 0]$ yields

$$\frac{PR^3}{\kappa} = \frac{\sigma R^2}{\kappa} - \frac{1}{2} - \frac{a\Phi^2 R^2}{2\kappa} - \frac{\Lambda \Phi R}{2\kappa}, \tag{5}$$

where we used Eq. (4) to eliminate $\mu$. While the first two terms on the right-hand side of Eq. (5) represent the conventional Laplace pressure, the last two are new and specific to our model problem. Note that by fixing the tube length $L$, we assume to have (indirect) control over the membrane tension $\sigma$. By contrast, the pressure $P$ adjusts itself for given $R$, $\sigma$, and other parameters according to Eq. (5).

Finally, the Hessian determinant of $F$ must be positive for the tube to be stable. This amounts to $[(\partial^2 F/\partial\phi^2)(\partial^2 F/\partial r^2) - (\partial^2 F/\partial\phi\partial r)^2]_{R,\Phi} > 0$, giving

$$\frac{PR^3}{\kappa} < 1 - \frac{\Lambda^2}{4\kappa a}. \tag{6}$$

From Eqs. (5) and (6), we conclude that the coated cylinder is stable if

$$\frac{\sigma R^2}{\kappa} < \frac{3}{2} + \frac{a\Phi^2 R^2}{2\kappa} + \frac{\Lambda \Phi R}{2\kappa} - \frac{\Lambda^2}{4\kappa a}. \tag{7}$$

Equation (7) generalizes a well-known stability criterion $\sigma R^2/\kappa < 3/2$ for uncoated membrane tubes [11,18–20], adding three terms related to the attached proteins. Summarizing, for given $\sigma$, $\Lambda$, $\mu$, and $a$, a tube of constant radius $R$ has a coat of density $\Phi$ [Eq. (4)] and a pressure drop $P$ [Eq. (5)] across its membrane.

### C. Linear stability analysis

To study what happens to the tube if Eq. (7) is not satisfied, we now consider a tube with slight undulations in its radius and coat density, $r(z) = R + u(z)$ and $\phi(z) = \Phi + \varphi(z)$, with $u(z) \ll R$ and $\varphi(z) \ll \Phi$ (see Fig. 1). We use that $\sqrt{g} = r\sqrt{1+(\partial_z r)^2}$, with $g$ being the metric determinant and $\partial_z = \partial/\partial z$, and that [12,20,71]

$$2H = \frac{1}{\sqrt{1+(\partial_z r)^2}}\left[\frac{\partial_z^2 r}{1+(\partial_z r)^2} - \frac{1}{r}\right]. \tag{8}$$

From hereon, we use the following dimensionless variables and parameters: $\bar{F} = F/(2\pi\kappa)$, $\bar{z} = z/R$, $\bar{L} = L/R$, $\bar{r} = r/R$, $\bar{\phi}(z) = \phi/\Phi$, $\bar{\sigma} = \sigma R^2/\kappa$, $\bar{P} = PR^3/\kappa$, $\bar{\Lambda} = \Lambda\Phi R/\kappa$, $\bar{a} = a\Phi^2 R^2/\kappa$, $\bar{\mu} = \mu\Phi R^2/\kappa$, and $\bar{b} = b\Phi^2/\kappa$. We can then express $\bar{F} = \bar{F}_H + \bar{F}_\phi$ as

$$\bar{F}_H = \frac{1}{2}\int_0^{\bar{L}} d\bar{z}\left\{\frac{\bar{r}}{\sqrt{1+(\partial_{\bar{z}}\bar{r})^2}}\left[\frac{\partial_{\bar{z}}^2\bar{r}}{1+(\partial_{\bar{z}}\bar{r})^2} - \frac{1}{\bar{r}}\right]^2 + 2\bar{\sigma}\bar{r}\sqrt{1+(\partial_{\bar{z}}\bar{r})^2} - \bar{P}\bar{r}^2\right\}, \tag{9a}$$

$$\bar{F}_\phi = \frac{1}{2}\int_0^{\bar{L}} d\bar{z}\left\{-\bar{\Lambda}\bar{\phi}\left[\frac{\bar{r}\partial_{\bar{z}}^2\bar{r}}{1+(\partial_{\bar{z}}\bar{r})^2} - 1\right] + \bar{r}\sqrt{1+(\partial_{\bar{z}}\bar{r})^2}[-2\bar{\mu}\bar{\phi} + \bar{a}\bar{\phi}^2 + \bar{b}(\partial_{\bar{z}}\bar{\phi})^2]\right\}. \tag{9b}$$

For tubes with radii around $R \approx 4\,\mu$m, we have $\bar{\sigma} \approx 1$. For the other dimensionless parameters, $\bar{a}$, $\bar{b}$, and $\bar{\Lambda}$, we will consider values around 1; see Appendix A.

Next, we expand the perturbations $\bar{u}(\bar{z}) = u/R$ and $\bar{\varphi}(\bar{z}) = \varphi/\Phi$ into Fourier modes,

$$\bar{u} = \sum_{\bar{q}\neq 0} \bar{u}_{\bar{q}} e^{i\bar{q}\bar{z}}, \quad \bar{\varphi} = \sum_{\bar{q}\neq 0} \bar{\phi}_{\bar{q}} e^{i\bar{q}\bar{z}}, \tag{10}$$

where $\bar{q} = 2\pi n/\bar{L}$ are dimensionless wave numbers (with $n \in \mathbb{N}$) and where $\bar{u}_{\bar{q}}$ and $\bar{\phi}_{\bar{q}}$ are the amplitudes of the modes. In Appendices C and D we insert Eq. (10) and $\bar{P}$ from Eq. (5) into $\bar{F}_H$ and $\bar{F}_\phi$. Retaining quadratic terms, we find

$$\bar{F} = \frac{\bar{L}}{4}\sum_{\bar{q}\neq 0}(\bar{u}_{\bar{q}}\ \bar{\phi}_{\bar{q}}) \underbrace{\begin{bmatrix} 2\bar{q}^4 + \zeta_2\bar{q}^2 + \zeta_0 & \bar{\Lambda}(\bar{q}^2-1) \\ \bar{\Lambda}(\bar{q}^2-1) & 2(\bar{a}+\bar{b}\bar{q}^2)\end{bmatrix}}_{\equiv B} \begin{pmatrix}\bar{u}_{-\bar{q}} \\ \bar{\phi}_{-\bar{q}}\end{pmatrix}, \tag{11}$$

with $\zeta_2 = \bar{\Lambda} - \bar{a} + 2\bar{\sigma} - 1$ and $\zeta_0 = \bar{\Lambda} + \bar{a} - 2\bar{\sigma} + 3$.

In Appendix E we consider Eq. (11) in the flat membrane limit $R \to \infty$ and find a leading-order contribution at $\mathcal{O}(R^2)$ coinciding with the free energy of a ruffled membrane sheet, studied previously by Leibler [51]. Away from this limit, however, Eq. (11) is much more involved, the chief reason lying in the different expansions of the square root of the metric determinant: a sheet with small ruffles of height $h$ yields, in the Monge parametrization, $\sqrt{g} \approx 1 + (\nabla h)^2/2 + \mathcal{O}(h^3)$; the ruffled tube in arc-length parametrization yields $\sqrt{g} = r\sqrt{1+(\partial_z r)^2} \approx R + u + R(\partial_z u)^2/2 + \mathcal{O}(u^3)$ instead. The presence of terms linear in the perturbation in the arc-length parametrization (and their absence in the Monge parametrization) precipitates in many more terms at quadratic order in the analysis of the membrane tube.

The stability of the coated membrane tube is governed by the smallest eigenvalue $\lambda_- = \mathrm{Tr}(B)/2 - \sqrt{\mathrm{Tr}(B)^2/4 - \det(B)}$ of $B$ [Eq. (11)], where $\mathrm{Tr}(B)$ and $\det(B)$ are the trace and determinant of $B$. When $\lambda_- < 0$, the system is unstable to a combination of density and radius perturbations set by the elements of the corresponding eigenvector. Figures 2(a) and 2(b) show $\lambda_-$ for $\bar{a} = 0.1$, $\bar{b} = 0.05$, $\bar{\sigma} = 0.5$, and several protein-curvature couplings $\bar{\Lambda}$ as indicated. We observe local minima at $\bar{q} = 0$ for all considered $\bar{\Lambda}$ and for finite $\bar{q}$ in a few cases; these minima appear, depending on $\bar{\Lambda}$, both at positive and negative $\lambda_-$ values. We discern four cases: For $\bar{\Lambda} = 0.5$, $\lambda_- > 0$ for all $q$ (case I); for $\bar{\Lambda} = 1.0$, $\lambda_-$ is negative only around $q = 0$ (case II); for $\bar{\Lambda} = 1.8$ and 2.3, $\lambda_-$ has a negative global minimum at $q = 0$ and a negative local minimum for $q \neq 0$ (case III); and for $\bar{\Lambda} = 2.6$, $\lambda_-$ has a negative global minimum at $q \neq 0$ and a negative local minimum for $q = 0$ (case IV). In Fig. 2(c), we characterize $\lambda_-$ according to the above cases in the plane of $\bar{\sigma}$ and $\bar{\Lambda}$. At the boundary between cases I and II, the minimum of $\lambda_-$ at $\bar{q} = 0$ crosses zero; $\lambda_- = 0$ requires $\det(B) = 0$, which, after setting $\bar{q} = 0$ in $B$, gives the stability criterion Eq. (7) in dimensionless form, $2\bar{\sigma} = (3 + \bar{a} + \bar{\Lambda} - \bar{\Lambda}^2/2\bar{a})$. We indicate this analytical result with a red dotted line. It would be interesting also to characterize the boundary between cases II and III, where the local minimum of

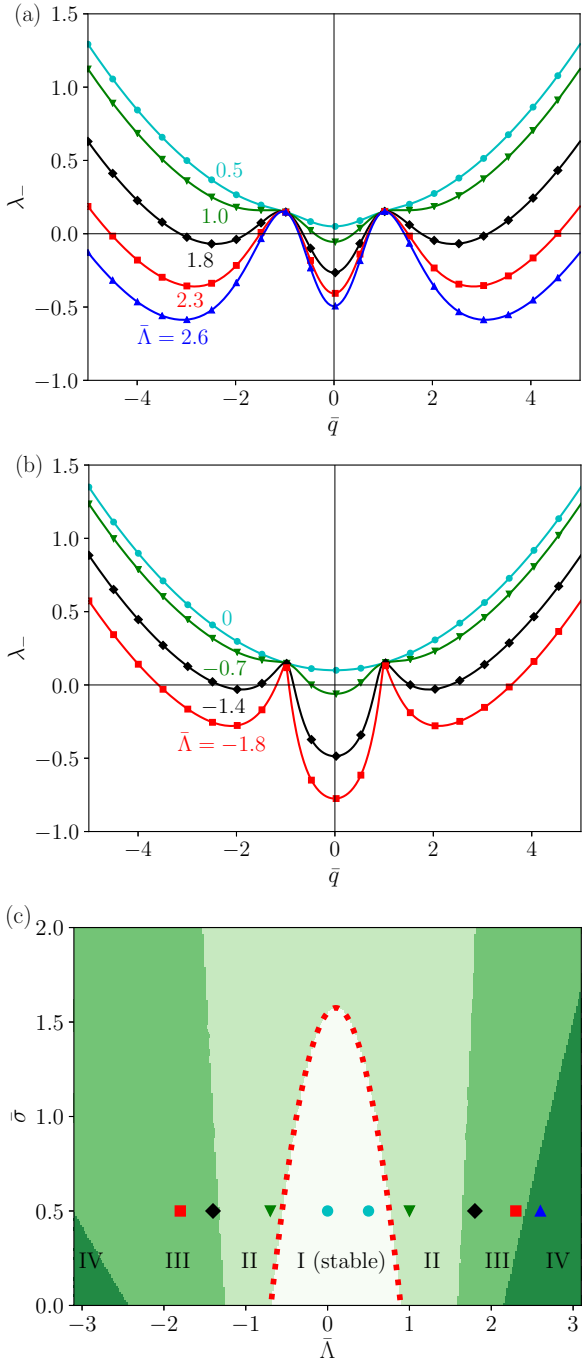


FIG. 2. The smallest eigenvalue $\lambda_-$ of $B$ [Eq. (11)] for $\bar{a} = 0.1$, $\bar{b} = 0.05$, $\bar{\sigma} = 0.5$, and $\bar{\Lambda} = [0.5, 1.0, 1.8, 2.3, 2.6]$ (a) and $\bar{\Lambda} = [0.0, -0.7, -1.4, -1.8]$ (b). We discern four types of minima of $\lambda_-$, which we denote with I, where $\lambda_- > 0$ for all $q$; II, where $\min(\lambda_-) < 0$ at $q = 0$ is the only minimum for which $\lambda_- < 0$; III, same as II, but with a secondary minimum for which $\lambda_- < 0$ for $q \neq 0$; and IV, where $\min(\lambda_-) < 0$ at $q \neq 0$. In panel (c), we characterize the minima of $\lambda_-$ according to these four cases in the plane of $\bar{\sigma}$ and $\bar{\Lambda}$. Symbols correspond to the parameter settings used in panels (a) and (b). The red dotted line represents Eq. (7).

$\lambda_-$ at $\bar{q} \neq 0$ crosses zero, as this is the criterion for finite-wavelength undulations to become unstable. In this case, $\det(B) = 0$ is a sixth-order polynomial in $\bar{q}$ containing only even powers of $\bar{q}$, which can thus be written as a cubic

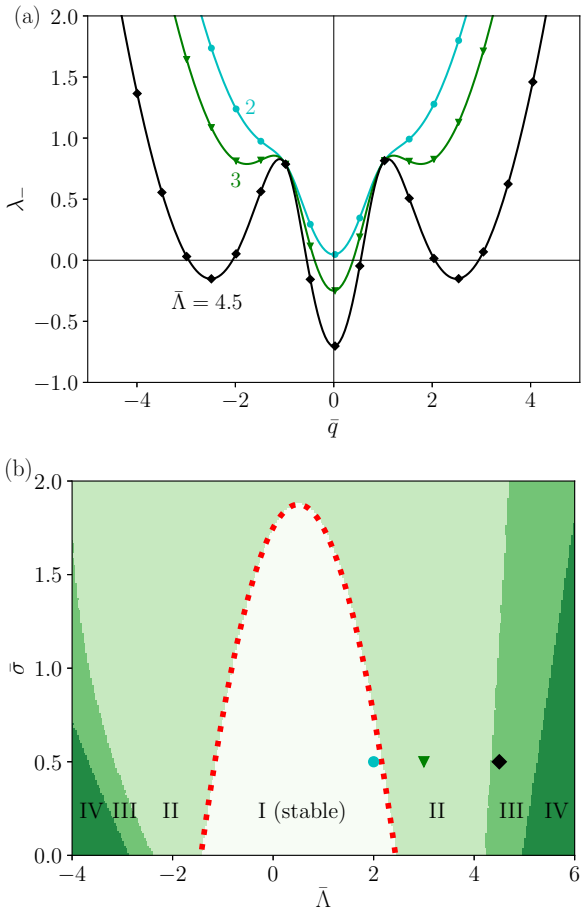


FIG. 3. (a) The smallest eigenvalue $\lambda_-$ of $B$ [Eq. (11)] for $\bar{a} = 0.5$, $\bar{b} = 0.3$, $\bar{\sigma} = 0.5$, and $\bar{\Lambda} = [2.0, 3.0, 4.5]$. In panel (b), we characterize the minima of $\lambda_-$ according to the same criteria as in Fig. 2. The red dotted line represents Eq. (7).

polynomial, $\det(B) = \alpha x^3 + \beta x^2 + \gamma x + \delta$, with $x = \bar{q}^2$, $\alpha = \bar{b}$, $\beta = \bar{b}\zeta_2 + \bar{a} - \bar{\Lambda}^2/4$, $\gamma = \bar{a}\zeta_2 + \bar{b}\zeta_0 + \bar{\Lambda}^2/2$, and $\delta = \bar{a}\zeta_0 - \bar{\Lambda}^2/4$. Depending on the sign of the discriminant $\Delta = \beta^2\gamma^2 - 4\alpha\gamma^3 - 4\beta^3\delta - 27\alpha^2\delta^2 + 18\alpha\beta\gamma\delta$, $\det(B) = 0$ thus has either 1 (if $\Delta < 0$) or 3 (if $\Delta > 0$) real solutions. While these expressions allow us to express the stability of the protein-covered membrane analytically, the resulting expressions are not tractable.

In Fig. 3, we redraw Fig. 2 for the larger values $\bar{a} = 0.5$ and $\bar{b} = 0.3$. For larger $\bar{a}$, proteins repel each other stronger; for larger $\bar{b}$, gradients in their density are penalized stronger. In Fig. 3 we see that, compared to Fig. 2, these larger $\bar{a}$ and $\bar{b}$ values drive the $q \neq 0$ minima of $\lambda_-$ to larger $\bar{\Lambda}$; hence, they suppress the generation of undulations. When proteins repel each other stronger, the membrane thus needs to couple stronger to the proteins for instabilities to occur.

## III. HYDRODYNAMIC INSTABILITY

### A. Setup

Next we consider how hydrodynamics and protein mobility set the dynamics of the membrane instability discussed above. We consider a membrane $\mathcal{M} \subset \mathbb{R}^3$, locally isomorphic to $\mathbb{R}^2$,

whose tangent bundle and normal bundle are spanned by a local orthonormal triad, $\{\mathbf{e}_1, \mathbf{e}_2, \mathbf{N}\}$, where $\mathbf{N}$ is normal to the surface and $\mathbf{e}_{1,2}$ are the tangent basis. The surface embedding is defined by the Gauss-Codazzi relations and the shape operator $\mathbf{S} = -\nabla\mathbf{N}$, where $\nabla$ is the gradient operator on the membrane. The mean and Gaussian curvatures are defined by $2H = \mathrm{Tr}(\mathbf{S})$ and $K = \det(\mathbf{S})$. The membrane is assumed to move with a velocity $\mathbf{V} = \mathbf{v} + v_n\mathbf{N}$, to be incompressible, and to have a 2D membrane viscosity $\eta_m$. The ambient fluid is assumed to be an incompressible Stokes fluid with viscosity $\eta$.

We will derive general dynamical equations in geometric form from the following free energy:

$$\mathcal{F} = \int f\, dA = \int \left(2\kappa H^2 - \Lambda\phi H + \frac{a}{2}\phi^2 + \frac{b}{2}|\nabla\phi|^2\right) dA, \tag{12}$$

where $\Lambda$, $\kappa$, $a$, and $b$ are as defined in Eqs. (1) and (2). We omitted the surface tension, pressure, and chemical potential terms, which will be introduced as conjugate variables to the dynamical constraints. Varying Eq. (12) with respect to perturbations of the surface of the form $\mathbf{R} \to \mathbf{R} + \psi\mathbf{N} + \delta\mathbf{x}$, where $\delta\mathbf{x} \in T(\mathcal{M})$, we find

$$\begin{aligned}
\delta\mathcal{F} &= \int \delta f\, dA + \int f\, \delta dA \\
&= \int \left\{ 4\kappa\left[\frac{1}{2}\nabla^2\psi + \psi(2H^2 - K)\right]H \right. \\
&\quad - \frac{1}{2}\Lambda\phi\nabla^2\psi - \psi\Lambda\phi(2H^2 - K) \\
&\quad \left. + b\nabla\phi\cdot(\mathbf{N}(\nabla\psi)\cdot\nabla\phi - \psi\nabla\mathbf{N}\cdot\nabla\phi)\right\} dA \\
&\quad - \int 2H\left(2\kappa H^2 - \Lambda\phi H + \frac{a}{2}\phi^2 + \frac{b}{2}|\nabla\phi|^2\right) dA \\
&\quad - \int (-\Lambda H + a\phi + b\nabla^2\phi)\nabla\phi\cdot\delta\mathbf{x}\, dA.
\end{aligned} \tag{13}$$

On integration by parts, this gives a normal force,

$$\begin{aligned}
\mathbf{f}^{\mathrm{elastic}} = -\Big[&2\kappa\nabla^2 H + 4\kappa H(H^2 - K) - \frac{\Lambda}{2}\nabla^2\phi + \Lambda\phi K \\
&- b\nabla\phi\cdot\nabla\mathbf{N}\cdot\nabla\phi - a\phi^2 H - b|\nabla\phi|^2 H\Big]\mathbf{N} \\
&+ (a\phi + b\nabla^2\phi - \Lambda H)\nabla\phi,
\end{aligned} \tag{14}$$

whose first part is the standard shape equation for an isotropic fluid membrane with purely bending energy [14]. For simplicity, we neglect the tangential elastic forces here.

To derive the full dynamical equations, we will consider a Rayleigh dissipation functional,

$$\mathcal{R} = \mathcal{P}^{\mathrm{bulk}} + \mathcal{P}^{\mathrm{mem}} + \mathcal{P}^{\mathrm{constraints}} + \int \frac{\delta\mathcal{F}}{\delta\mathbf{R}}\cdot\mathbf{V}\, dA, \tag{15}$$

where $\mathbf{V} = d\mathbf{R}/\,dt$ is the surface velocity of the membrane. Moreover, $\mathcal{P}^{\mathrm{bulk}}$ is the dissipation functional of the bulk fluid, $\mathcal{P}^{\mathrm{mem}}$ is the dissipation functional of the membrane, and $\mathcal{P}^{\mathrm{constraints}}$ is the dissipation functional associated with constraints on the system dynamics, in our case, fluid and membrane incompressibility and protein conservation.

The bulk dissipation is defined by

$$\mathcal{P}^{\mathrm{bulk}} = \int \eta\mathcal{D} : \mathcal{D}\, dV, \tag{16}$$

where $\mathcal{D} = [\vec{\nabla}\vec{V} + (\vec{\nabla}\vec{V})^T]/2$ is the stain rate in the ambient fluid, where $\vec{\nabla}$ is the gradient operator in $\mathbb{R}^3$ and $\vec{V}$ is the velocity field of the ambient fluid. The associated constraint imposing bulk incompressibility is

$$\mathcal{P}^{\mathrm{bulk.const.}} = \int P\vec{\nabla}\cdot\vec{V}\, dV, \tag{17}$$

where $P$ is the hydrodynamic pressure.

Equivalently, for the membrane with surface velocity $\mathbf{V} = \mathbf{v} + v_n\mathbf{N}$, we have

$$\mathcal{P}^{\mathrm{mem}} = \int \eta_m D : D\, dA, \tag{18}$$

where $D = \mathbb{P}\cdot[\nabla\mathbf{V} + (\nabla\mathbf{V})^T]\cdot\mathbb{P}/2 = 1/2(\nabla^\alpha v^\beta + \nabla^\beta v^\alpha - S^{\alpha\beta}v_n)\mathbf{e}_\alpha\mathbf{e}_\beta$ is the surface deformation rate. Here $\mathbb{P} = \mathbb{I}_3 - \mathbf{NN}$ is the projection operator onto the tangent space of the membrane from $\mathbb{R}^3$. For the surface incompressibility, we have

$$\mathcal{P}^{\mathrm{mem.const.}} = -\int \sigma\nabla\cdot\mathbf{V}\, dA = -\int \sigma(\nabla_\alpha v^\alpha - 2Hv_n)\, dA, \tag{19}$$

where $\sigma$ is the hydrodynamic surface tension.

Additionally, we impose local conservation of proteins by the dynamical constraint functional

$$\mathcal{P}^{\phi} = \int \mu\left[\partial_t\phi + \nabla\cdot\left(\mathbf{V}\phi - \mathbf{M}\cdot\nabla\frac{\delta\mathcal{F}}{\delta\phi}\right)\right] dA, \tag{20}$$

where $\mu$ is the chemical potential of the proteins on the surface and $\mathbf{M}$ is the protein mobility tensor on the surface. For simplicity, we assume $\mathbf{M} = M\mathbb{I}_2$, with $M$ being the protein mobility on the surface. Note that in Sec. II, the chemical potential regulated the exchange of proteins from the membrane to its liquid environment. In Eq. (20), the dynamics of the proteins on the membrane are assumed much faster than the exchange of proteins between the membrane and the liquid.

Taking functional derivatives of the Rayleigh dissipation functional $\mathcal{R}$ [Eq. (15)] with respect to the ambient fluid velocity $\vec{V}$ and pressure $P$ now yields the Stokes and mass conservation equations of the ambient fluid,

$$\eta\vec{\nabla}^2\vec{V} = \vec{\nabla}P, \tag{21a}$$

$$\vec{\nabla}\cdot\vec{V} = 0. \tag{21b}$$

Likewise, $\delta\mathcal{R}/\delta\sigma = 0$ gives the incompressibility equation of the membrane,

$$\nabla\cdot\mathbf{V} = \nabla\cdot\mathbf{v} - 2Hv_n = 0, \tag{22}$$

and $\delta\mathcal{R}/\delta\mathbf{V} = 0$ gives the surface force balance

$$-\left[2\kappa\nabla^2 H + 4\kappa H(H^2 - K) - \frac{\Lambda}{2}\nabla^2\phi + \Lambda\phi K + b\nabla\phi\cdot\mathbf{S}\cdot\nabla\phi - a\phi^2 H - b|\nabla\phi|^2 H\right]\mathbf{N} + \nabla\sigma + 2H\sigma\mathbf{N} - \phi\nabla\mu - 2H\mu\phi\mathbf{N}$$
$$+ \eta_m\{\nabla_\parallel\cdot[\nabla_\parallel\mathbf{v} + (\nabla_\parallel\mathbf{v})^T] - 4v_n\nabla H - 2\mathbf{S}\cdot\nabla v_n\} + 2\eta_m[\nabla_\parallel\mathbf{v} : (\mathbf{S} - H\mathbb{I}_2) - 2v_n(H^2 - K)]\mathbf{N}$$
$$= \eta[\mathcal{D}]\cdot\mathbf{N} - [P]\mathbf{N}, \tag{23}$$

where $\nabla_\parallel\mathbf{v} = \nabla\mathbf{v} - (\nabla\mathbf{v}\cdot\mathbf{N})\mathbf{N}$ is the covariant derivative of $\mathbf{v}$. The tangential part of this is the covariant Stokes equation, and the normal part corresponds to the shape equation (including viscous stresses). $[\mathcal{D}]$ is the jump in the ambient deformation rate tensor across the membrane.

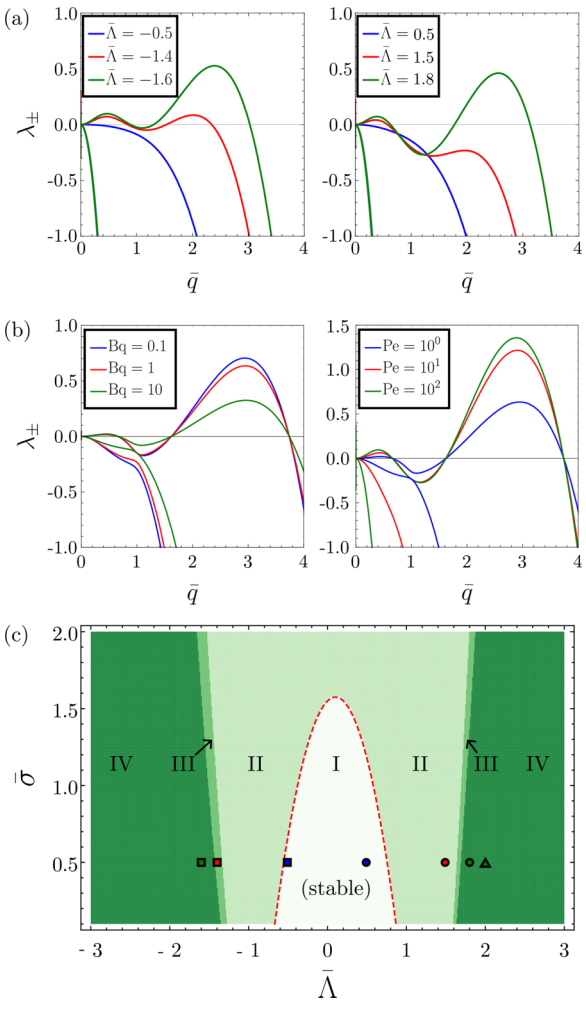


FIG. 4. Eigenvalues $\lambda_\pm$ of the dynamical stability matrix $\tilde B$ [Eq. (25b)] for Bq = 1, Pe = $10^2$, and various $\bar\Lambda$ (a) and for $\bar\Lambda = 2$ and various Bq and Pe (b). Throughout, $\bar a = 0.1$, $\bar b = 0.05$, and $\bar\sigma = 0.5$. Panel (c) shows a stability diagram for Bq = 1 and Pe = $10^2$, with regions defined as in Fig. 2. The red dotted line represents Eq. (7), the squares and circles correspond to the curves from panel (a) (left and right, respectively), and the triangle corresponds to the green curve in the right panel of (b).

Finally, $\delta\mathcal{R}/\delta\mu = 0$ gives a continuity equation for the protein concentration,

$$\partial_t\phi + \mathbf{v}\cdot\nabla\phi - aM\nabla^2\phi + \Lambda M\nabla^2 H + bM\nabla^4\phi = 0, \tag{24}$$

where $\partial_t = \partial/\partial t$. Equations (22)–(24) are coordinate-free versions of the equations of irreversible thermodynamics of fluid bilayers derived in Ref. [29], assuming the entropy of mixing term is expanded to quadratic order. They are closed by no-slip and no-permeation boundary conditions between the ambient fluid and membrane.

### B. Stability analysis

We consider an axisymmetric tube with radius $r = R + u(z,t)$ and protein concentration $\phi = \Phi + \delta\Phi(z,t)$ and, in Appendix F, expand Eqs. (22)–(24) and the boundary conditions of Eq. (21) out to linear order in the perturbations $u(z,t)$ and $\delta\Phi(z,t)$. Transforming to Fourier space and solving for velocities of the bulk flow and membrane, surface tension variation, and pressures then gives

$$\partial_{\bar t}\begin{pmatrix}\bar u_q\\ \delta\bar\phi_q\end{pmatrix} = \tilde B\begin{pmatrix}\bar u_q\\ \delta\bar\phi_q\end{pmatrix}, \tag{25a}$$

where

$$\tilde B = -\begin{bmatrix}\dfrac{2\bar q^4 + \zeta_2\bar q^2 + \zeta_0}{4(\beta + 2\mathrm{Bq})} & \dfrac{\bar\Lambda(\bar q^2 - 1)}{4(\beta + 2\mathrm{Bq})}\\ \dfrac{\mathrm{Pe}}{2}\bar\Lambda(\bar q^4 - \bar q^2) & \mathrm{Pe}(\bar a\bar q^2 + \bar b\bar q^4)\end{bmatrix} \tag{25b}$$

and

$$\beta = (\bar q^2 + 1)[I_0(\bar q)K_1(\bar q) - I_1(\bar q)K_2(\bar q)]$$
$$\times\{\bar q[\bar q I_0(\bar q)^2 - 2I_1(\bar q)I_0(\bar q) - \bar q I_1(\bar q)^2]$$
$$\times[\bar q K_0(\bar q)^2 + 2K_1(\bar q)K_0(\bar q) - \bar q K_1(\bar q)^2]\}^{-1}. \tag{25c}$$

Here time has been nondimensionalized by $\bar t = t/\tau$, with $\tau = \eta R/\kappa$, and $I_m(x)$ and $K_m(x)$ are modified Bessel functions of the first and second kind, respectively. The Péclet number $\mathrm{Pe} = M\eta/R^3\Phi^2$ compares surface mobility to bulk viscous advection. The Boussinesq number $\mathrm{Bq} = \eta_m/(R\eta)$ contains a ratio of membrane viscosity to bulk viscosity. In the context of membranes, the Boussinesq number is sometimes called the Saffman-Delbrück number. With $\eta = 10^{-3}$ Pa s, $\eta_m = 10^{-9}$ Pa m s [72], $D = 10^{-12}$ m$^2$ s$^{-1}$ [73] (which gives

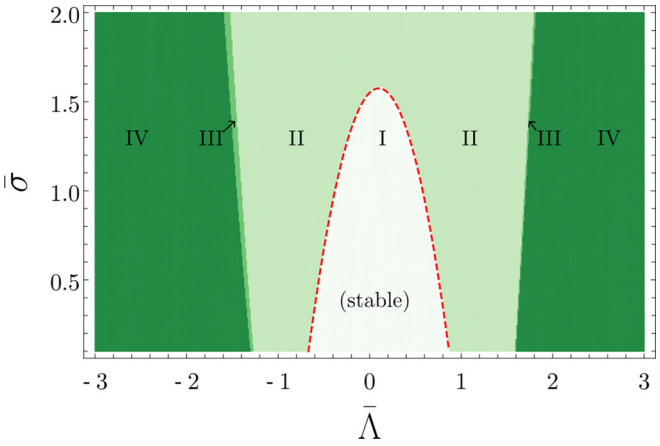


FIG. 5. Stability plot for Pe = 1; all other values are identical to Fig. 4(c).

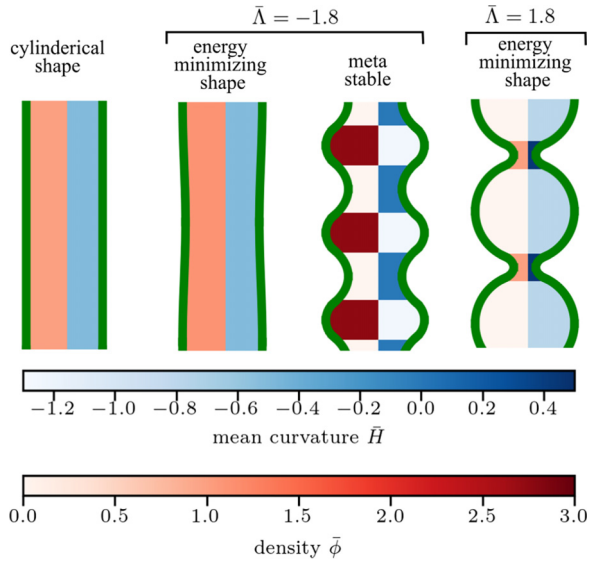


FIG. 6. Membrane tube shape: The cylindrical shape has a constant mean curvature $\bar{H} = RH$, with $= -1/2$ and a constant protein density $\bar{\phi} = 1$. The areal protein density and mean curvature of the undulating shapes are shown as color maps. We use $\bar{\sigma} = 0.5$, $\bar{a} = 0.1$, and $\bar{b} = 0.05$ in all panels.

access to $M = D/a$), and $R \approx 6 \times 10^{-8}$ m [see Appendix A], we estimate Pe $\gg 1$ and Bq $\sim 1$ (see also Ref. [74]). All other dimensionless quantities are as defined in Sec. II C. Note that the stability matrix $\tilde{B}$ in Eq. (25b) is similar to $B$ [Eq. (11)] as derived from the free energy (up to an overall minus sign), only with dissipative prefactors multiplying each row. Moreover, $\tilde{B}$ is similar to the stability matrix of a flat membrane [45] [see also Eq. (B17)] but also accounts for membrane viscosity.

To understand how hydrodynamics affects the wavelength selection of the instability, we plot the eigenvalues $\lambda_\pm$ of the stability matrix $\tilde{B}$ (i.e., the growth rate) in Fig. 4(a) for Pe $= 10^2$ Bq $= 1$ and several protein curvature couplings $\bar{\Lambda}$. We note that, for $\tilde{B}$, positive $\lambda_\pm$ corresponds to instability, whereas the opposite is true for $B$. We see that the bulk hydrodynamics screens the small $\bar{q}$ instability as the confinement of the tube gives an infinite resistance to the pearling mode in the long-wavelength limit. The small-$\bar{q}$ mode grows essentially as a classical pearling instability with its wavelength set by the Boussinesq number [74]; see Fig. 4(b). The wavelength of the large $\bar{q}$ instability is relatively unchanged as the membrane dissipation controls the dissipative dynamics. Here the length scale is essentially set by the elastic forces derived from the free energy, while the dynamical parameters control the growth rate; see Fig. 4(b). We note that for large Péclet number, the growth rate saturates to a value controlled by the membrane viscosity. Last, Fig. 4(c) shows a stability diagram similar to Fig. 2(c), now based on hydrodynamic theory. We see that the main characteristics of the instability are unchanged. Region III, where both high and low $\bar{q}$ are unstable, is significantly reduced by bulk hydrodynamics. Moreover, the short wavelength instability quickly becomes the fastest-growing mode; see Fig. 4(c).

Figure 5 shows a stability diagram for a smaller value Pe $= 1$ of the Péclet number. We see that varying Pe hardly changes the stability diagram as compared to Fig. 4(c), except for a slightly smaller region III with a subdominant $q \neq 0$ instability.

The similarities between the stability diagrams of Figs. 2, 4, and 5 suggest that the free-energy calculations of Sec. II capture the general wavelength selection mechanisms for the dominant high $\bar{q}$ instability. Thus, we proceed with a purely energetic analysis in Sec. IV to determine the membrane's shape beyond the onset of the instability.

## IV. ENERGY MINIMIZING SHAPE

Finally, we discuss the membrane shape beyond the onset of the instability. Note that the $\bar{b}|\nabla\phi|^2/2$ term in Eq. (2) promotes a homogeneous protein coat. This term acts as an effective line tension $\gamma$ in the case of strong density gradients between dense $[\bar{\phi} = \bar{\phi}^{(\mathrm{I})}]$ and dilute $[\bar{\phi} = \bar{\phi}^{(\mathrm{II})}]$ protein domains, where we estimate $\gamma = \sqrt{2\bar{b}\bar{\sigma}}[\bar{\phi}^{(\mathrm{I})} - \bar{\phi}^{(\mathrm{II})}]$ (see Appendix G). Therefore, we limit the discussion of tube shapes to cases where the tube is covered either by a continuous protein coat or by alternating homogeneous domains of dilute and dense coats. In the latter case, the line tension $\gamma$ acts at the interface between the dilute and dense domain. In Appendix G, we derive the shape equation for tube domains with a homogeneous protein coat [Eq. (G3)] and discuss its solutions for different membrane-protein interactions $\bar{\Lambda}$. Within such homogeneous domains, the shape equation is solved by shapes with constant mean curvature, so-called Delaunay shapes [75]. For all shapes discussed here, the volume is conserved.

Figure 6 shows examples of the tube shapes for $\bar{\Lambda} = -1.8$ and $\bar{\Lambda} = 1.8$. For $\bar{\Lambda} = -1.8$, the lowest-energy shape is a weak undulation with a continuous homogeneous protein coat with a slightly higher protein density than the reference cylindrical shape. We note that there is a second solution to the shape equation characterized by an alternation of protein-free and protein-dense domains. The corresponding change in mean curvature ($\bar{H} = 0$ in the protein-free domain and $\bar{H} = \bar{\Lambda}\bar{\phi}/4$ in the dense domain, with $\bar{H} = RH$) leads to a strong undulation. The energy of this tube shape is lower

than that of a cylinder but higher than that of the previously discussed weak undulation with a homogeneous protein coat.

For $\bar{\Lambda} = 1.8$, the shape of a tube cannot be described by a constant and positive mean curvature. Therefore, we do not find a solution to the shape equations for a continuous protein coat for this case. The energy-minimizing shapes exhibit large undulations with extended protein-free regions. In contrast to the tube shapes for $\bar{\Lambda} = -1.8$, where regions with negative mean curvature exhibit a large protein density, we find the regions with negative mean curvature to be protein free.

We note the undulating shapes found in Fig. 6 and anticipated in Fig. 2 are characteristic of the small $\bar{a}$ and $\bar{b}$ used there. In Fig. 3(c), we showed a stability diagram for larger $\bar{a}$ and $\bar{b}$. The negative local minima for $\bar{q} \neq 0$ appeared in that diagram only at correspondingly stronger protein-membrane interaction parameters $\bar{\Lambda}$. Physically, particles will destabilize a membrane tube only if they interact strongly with it, but weakly among themselves.

## V. CONCLUSION

We studied the stability of a membrane tube coated with proteins. By a linear stability analysis, we identified short and long-wavelength instabilities that we corroborated by hydrodynamic theory and through numerical calculations. Our analysis showed that both membrane and protein properties determine the onset of shape instabilities; proteins thus have a regulatory effect on the shape and stability of membrane tubes. Moreover, our model revealed an interplay between membrane shape and protein density: The membrane shape instability studied here concurred with a redistribution of proteins into a banded pattern. Last, our hydrodynamic model identified a bimodal instability in protein-covered tubules, which has not been reported yet in this context. We hope these results inspire further experiments on the interplay between tubules and their adhering proteins. Moreover, future work may extend our analysis to tubes relaxing assumptions of cylindrical symmetry, considering asymmetry in spontaneous protein curvature [43] and allowing for activity of the proteins due to ATP- or GTP-induced conformational changes [20,42].

## ACKNOWLEDGMENTS

We thank David Andelman, Andrew Callan-Jones, Markus Deserno, and Gareth Alexander for insightful discussions. The research leading to these results has received funding from the European Union's Horizon 2020 research and innovation programme under the Marie Skłodowska-Curie Grant No. 801133. M.J. was supported by an Advanced Grant from the European Research Council (Grant No. 788954). S.C.A. was supported by funding from the European Union's Horizon Europe research and innovation programme under the Marie Skłodowska-Curie postdoctoral fellowship No. 101106384.

There are no conflicts to declare.

## APPENDIX A: PARAMETER ESTIMATES

We make the following parameter estimates:

(1) $\Phi \approx 3 \times 10^{15}\,\mathrm{m}^{-2}$. For this order of magnitude estimate, we considered 5% of the area of the membrane tube to be covered by proteins. The protein area of one protein is taken to be $15\,\mathrm{nm}^2$. This means we have 1 protein per $200\,\mathrm{nm}^2$ $\approx 3.33 \times 10^{15}\,\mathrm{m}^{-2}$.

(2) We are not aware of experimental data for $a$; we estimate $a \approx 2 \times 10^{-36}\,\mathrm{J\,m}^2$. This estimate is based on methods of Ref. [45]: Below Eq. (B15) we show that our $a$ corresponds to their $\kappa/(R^2\Phi^2) + \cancel{(4T - J)/(a^2\Phi^2)}$, the latter term vanishing because they set $J = 4T$. Next, we use $a = \kappa/(R^2\Phi^2)$ and values for $\kappa$ and $\Phi$ to estimate $R$ (see Item 3 below). Inserting that $R$ estimate gives $a \approx 2.04 \times 10^{-36}\,\mathrm{J\,m}^2$.

(3) We estimate $R \approx 6 \times 10^{-8}\,\mathrm{m}$ by solving Eq. (5) for $R$, using $P = 0$, the $\Phi$ value estimated above, $\kappa = 20 k_B T$ [68], and $a = \kappa/(R^2\Phi^2)$, see Item 2. This $R$ value is slightly larger than the predicted radius $R = \sqrt{\kappa/(2\sigma)} \approx 4.5 \times 10^{-8}\,\mathrm{m}$ for an uncoated membrane tube.

(4) To estimate $\Lambda$, we note that the $-\Lambda\phi H$ term in Eq. (2) corresponds to $-4\kappa H H_0$ of Ref. [48]. Here $H_0$ is spontaneous curvature induced by proteins. Assuming $H_0$ to be linearly dependent on the protein density, we take $H_0 \to H_0\Phi/\Phi_{\max}$, with $\Phi_{\max}$ the protein density at close packing, which we take to be around a packing fraction of 0.5, so $\Phi_{\max} \approx 3.3 \times 10^{16}\,\mathrm{m}^{-2}$; see Item 1. We set $\phi \to \Phi$ and rewrite to $\Lambda = 4\kappa H_0/\Phi_{\max}$. Inserting $\Phi_{\max}$ and $\kappa$ and estimating the spontaneous curvature by $H_0 \approx 10^{-7}\,\mathrm{m}^{-1}$, we find $\Lambda \approx -9.71 \times 10^{-29}\,\mathrm{J\,m}$.

Using the above estimates and data of Sec. II for the values for $R, \kappa, \sigma, a, \Phi$, and $\Lambda$, we find $\bar{\sigma} = 0.9$, $\bar{a} = 1$, $\bar{\Lambda} = -0.24$. Due to the uncertainties in all the dimensional variables, we chose to vary all dimensionless parameters around 1.

## APPENDIX B: STABILITY OF A FLAT PROTEIN-COVERED MEMBRANE

We consider the same free energy $F = F_H + F_\phi$ as in Eqs. (1) and (2) and revisit the stability of a flat protein-covered membrane sheet. In the Monge parametrization [12], considering slight deviations $h(\mathbf{x})$ from a flat membrane, we have $dA = (1 + \frac{1}{2}(\nabla h)^2)\, d\mathbf{x}$ and $H = \frac{1}{2}\nabla^2 h$, where $\boldsymbol{\nabla}$ is the gradient operator. This yields

$$F = \frac{1}{2}\int d\mathbf{x}\left[1 + \frac{1}{2}(\nabla h)^2\right]\{2\sigma + \kappa(\nabla^2 h)^2 - \Lambda\phi(\nabla^2 h) - 2\mu\phi + a\phi^2 + b(\nabla\phi)^2\}. \tag{B1}$$

Inserting

$$h(\mathbf{x}) = \sum_{\mathbf{q}\neq\mathbf{0}} h_{\mathbf{q}} e^{i\mathbf{q}\cdot\mathbf{x}}, \tag{B2a}$$

$$\phi(\mathbf{x}) = \Phi + \sum_{\mathbf{q}\neq\mathbf{0}} \phi_{\mathbf{q}} e^{i\mathbf{q}\cdot\mathbf{x}} \equiv \Phi + \varphi(\mathbf{x}), \tag{B2b}$$

into Eq. (B1) yields

$$F = \frac{1}{2}\int d\mathbf{x}\left[1 - \frac{1}{2}\sum_{\mathbf{q},\mathbf{q}'\neq\mathbf{0}} \mathbf{q}\cdot\mathbf{q}' h_{\mathbf{q}} h_{\mathbf{q}'} e^{i(\mathbf{q}+\mathbf{q}')\cdot\mathbf{x}}\right]\Bigg\{2\sigma + \kappa \sum_{\mathbf{q},\mathbf{q}'\neq\mathbf{0}} q^2 (q')^2 h_{\mathbf{q}} h_{\mathbf{q}'} e^{i(\mathbf{q}+\mathbf{q}')\cdot\mathbf{x}} - \Lambda\left(\Phi + \sum_{\mathbf{q}\neq\mathbf{0}} \phi_{\mathbf{q}} e^{i\mathbf{q}\cdot\mathbf{x}}\right)\left[-\sum_{\mathbf{q}'\neq\mathbf{0}} (q')^2 h_{\mathbf{q}'} e^{i\mathbf{q}'\cdot\mathbf{x}}\right]$$
$$- 2\mu\left(\Phi + \sum_{\mathbf{q}\neq\mathbf{0}} \phi_{\mathbf{q}} e^{i\mathbf{q}\cdot\mathbf{x}}\right) + a\left[\Phi^2 + 2\sum_{\mathbf{q}\neq\mathbf{0}} \phi_{\mathbf{q}} e^{i\mathbf{q}\cdot\mathbf{x}} + \sum_{\mathbf{q},\mathbf{q}'\neq\mathbf{0}} \phi_{\mathbf{q}}\phi_{\mathbf{q}'} e^{i(\mathbf{q}+\mathbf{q}')\cdot\mathbf{x}}\right] - b\left[\sum_{\mathbf{q},\mathbf{q}'\neq\mathbf{0}} \mathbf{q}\cdot\mathbf{q}'\phi_{\mathbf{q}}\phi_{\mathbf{q}'} e^{i(\mathbf{q}+\mathbf{q}')\cdot\mathbf{x}}\right]^2\Bigg\}, \tag{B3}$$

with $q = |\mathbf{q}|$. We can partition the above expression as $F = F_0 + F_1 + F_2$, with $F_0 = \mathcal{O}(\epsilon^0)$, $F_1 = \mathcal{O}(\epsilon^1)$, $F_2 = \mathcal{O}(\epsilon^2)$, and $\epsilon$ shorthand for the perturbations $h_{\mathbf{q}}$ and $\phi_{\mathbf{q}}$. The $F_0$ term provides a constant offset to the free energy and can be ignored from hereon. The $F_1$ term does not contribute as it is of the form

$$F_1 = \int d\mathbf{x} \sum_{\mathbf{q}\neq\mathbf{0}} e^{i\mathbf{q}\cdot\mathbf{x}}[h_{\mathbf{q}}(\ldots) + \phi_{\mathbf{q}}(\ldots)]$$
$$= \sum_{\mathbf{q}\neq\mathbf{0}} \delta_{\mathbf{q},0}[h_{\mathbf{q}}(\ldots) + \phi_{\mathbf{q}}(\ldots)] = 0. \tag{B4}$$

Up to second order in the perturbations $h_{\mathbf{q}}$ and $\phi_{\mathbf{q}}$, we find

$$F = \frac{1}{2}\int d\mathbf{x} \sum_{\mathbf{q},\mathbf{q}'\neq\mathbf{0}} e^{i(\mathbf{q}+\mathbf{q}')\cdot\mathbf{x}}\Bigg\{\Bigg[\left(\mu\Phi - \sigma - \frac{a}{2}\Phi^2\right)\mathbf{q}\cdot\mathbf{q}'$$
$$+ \kappa q^2 (q')^2\Bigg] h_{\mathbf{q}} h_{\mathbf{q}'} + \Lambda (q')^2 \phi_{\mathbf{q}} h_{\mathbf{q}'}$$
$$+ (a - b\mathbf{q}\cdot\mathbf{q}')\phi_{\mathbf{q}}\phi_{\mathbf{q}'}\Bigg\}. \tag{B5}$$

Integrating over $\mathbf{x}$ gives

$$F = \frac{A}{2}\sum_{\mathbf{q}\neq\mathbf{0}}\Bigg\{\Bigg[\left(\sigma + \frac{a}{2}\Phi^2 - \mu\Phi\right)q^2 + \kappa q^4\Bigg] h_{\mathbf{q}} h_{-\mathbf{q}}$$
$$+ \Lambda q^2 \phi_{\mathbf{q}} h_{-\mathbf{q}} + (a + bq^2)\phi_{\mathbf{q}}\phi_{-\mathbf{q}}\Bigg\}, \tag{B6}$$

with $A$ the area of the membrane patch. With the Euler Lagrange equation $\delta F/\delta\phi = \nabla\cdot(\delta F/\delta\nabla\phi)$ we find $-\Lambda(\nabla^2 h) - 2\mu + 2a\phi = 2b\nabla^2\phi$. For a homogeneously coated flat membrane, this yields $\mu = a\Phi$. We can thus write Eq. (B6) in matrix form as

$$F = \frac{A}{2}\sum_{\mathbf{q}\neq\mathbf{0}} \begin{pmatrix} h_{\mathbf{q}} & \phi_{\mathbf{q}}\end{pmatrix}\begin{bmatrix} \kappa q^4 + \left(\sigma - \frac{a}{2}\Phi^2\right)q^2 & \frac{1}{2}\Lambda q^2 \\ \frac{1}{2}\Lambda q^2 & a + bq^2\end{bmatrix}$$
$$\times \begin{pmatrix} h_{-\mathbf{q}} \\ \phi_{-\mathbf{q}}\end{pmatrix}. \tag{B7}$$

For small $q$, the eigenvalues of the above matrix read

$$\lambda_- = \left(\sigma - \frac{a}{2}\Phi^2\right)q^2 + \left(\kappa - \frac{\Lambda^2}{4a}\right)q^4 + \mathcal{O}(q^5), \tag{B8}$$

$$\lambda_+ = a + bq^2 + \frac{\Lambda^2}{4a}q^4 + \mathcal{O}(q^5), \tag{B9}$$

from which we see that the flat membrane is unstable for $\sigma < a\Phi^2/2$. For the case $\sigma = a\Phi^2/2$, we recover the instability criterion $\kappa < \Lambda^2/(4a)$ of Ref. [51] [there is a factor 2 difference in our definitions of $\Lambda$, as Ref. [51] defines the mean curvature in terms of principle curvatures ($R_1$ and $R_2$) as $H = 1/R_1 + 1/R_2$, without a factor 2]. Equation (B8) implies the equilibrium height variance $\langle|h_{\mathbf{q}}|^2\rangle = k_B T/\lambda_-$, see Eqs. (8) and (9) of Ref. [42]. In other words, the long-wavelength height fluctuations diverge at the stated instability criterion.

In the above derivation, we followed Refs. [24–26], who included the $\sqrt{g} \sim 1 + \frac{1}{2}(\nabla h)^2$ prefactor for the $\phi$-dependent terms of $F$. In contrast, Refs. [22,23,30,42,51] multiplied the area element $\sqrt{g}$ only with the term proportional to $\sigma$, yielding

$$F = \frac{1}{2}\int d\mathbf{x}\,[\sigma(\nabla h)^2 + \kappa(\nabla^2 h)^2 - \Lambda\phi(\nabla^2 h)$$
$$- 2\mu\phi + a\phi^2 + b(\nabla\phi)^2], \tag{B10}$$

instead of Eq. (B1). Repeating the above derivation, we now find

$$F = \frac{A}{2}\sum_{\mathbf{q}\neq\mathbf{0}} \begin{pmatrix} h_{\mathbf{q}} & \phi_{\mathbf{q}}\end{pmatrix}\begin{pmatrix} \kappa q^4 + \sigma q^2 & \frac{1}{2}\Lambda q^2 \\ \frac{1}{2}\Lambda q^2 & a + bq^2\end{pmatrix}\begin{pmatrix} h_{-\mathbf{q}} \\ \phi_{-\mathbf{q}}\end{pmatrix}, \tag{B11}$$

and eigenvalues

$$\lambda_- = \sigma q^2 + \left(\kappa - \frac{\Lambda^2}{4a}\right)q^4 + \mathcal{O}(q^5), \tag{B12}$$

$$\lambda_+ = a + bq^2 + \frac{\Lambda^2}{4a}q^4 + \mathcal{O}(q^5). \tag{B13}$$

In this case, the flat membrane is unstable for $\sigma < 0$.

Finally, we compare the above expressions to the free energy of Veksler and Gov [45],

$$F = \int d\mathbf{x}\Bigg\{\frac{1}{2}(\sigma - \alpha\bar{\phi})(\nabla h)^2 + \frac{\kappa}{2}\left(\nabla^2 h + \frac{\bar{\phi}}{R}\right)^2$$
$$+ \frac{T}{a^2}[\bar{\phi}\ln\bar{\phi} + (1-\bar{\phi})\ln(1-\bar{\phi})]$$
$$+ \frac{J}{2a^2}\bar{\phi}(1-\bar{\phi}) + \frac{J}{4}(\nabla\bar{\phi})^2\Bigg\}, \tag{B14}$$

whose various parameters we will relate to those in Eq. (B1). Reference [45] considers Eq. (B14) around $\bar{\phi} = 1/2$, so we

substitute $\bar{\phi} \to 1/2 + \bar{\phi}$ and expand for small $\bar{\phi} \ll 1$, giving

$$F = F_0 + \frac{1}{2}\int d\mathbf{x}\left[\left(\sigma - \frac{\alpha}{2}\right)(\nabla h)^2 + \kappa(\nabla^2 h)^2 + \frac{2\kappa}{R}\bar{\phi}\nabla^2 h + \frac{\kappa}{R^2}\bar{\phi} + \left(\frac{\kappa}{R^2} + \frac{4T - J}{a^2}\right)\bar{\phi}^2 + \frac{J}{2}(\nabla\bar{\phi})^2 - \alpha\bar{\phi}(\nabla h)^2 + \frac{\kappa}{R}\nabla^2 h + \frac{2}{3}\frac{T}{a^2}\bar{\phi}^4\right], \tag{B15}$$

where $F_0$ is a constant offset to the free energy that we ignore from hereon. We see that the first two lines of Eq. (B15) coincide with Eq. (B10) if we take $\sigma \to \sigma - \alpha/2$, $\Lambda \to -2\kappa/(R\Phi)$, $\mu \to -\kappa/(2R^2\Phi)$, $a \to \kappa/(R^2\Phi^2) + (4T - J)/(a^2\Phi^2)$, and $b \to J/(2\Phi^2)$ in the latter expression. The third line of Eq. (B15) contains terms not in Eq. (B10). We can again substitute the Fourier represented perturbed height and protein density Eq. (B2), where we should set $\Phi = 0$ as we already assumed that $\bar{\phi} \ll 1$. This yields

$$F = \frac{1}{2}\int d\mathbf{x} \sum_{\mathbf{q},\mathbf{q}'\neq\mathbf{0}} e^{i(\mathbf{q}+\mathbf{q}')\cdot\mathbf{x}} \times \left\{\left[\left(\frac{\alpha}{2} - \sigma\right)\mathbf{q}\cdot\mathbf{q}' + \kappa q^2 (q')^2\right]h_{\mathbf{q}}h_{\mathbf{q}'} - \frac{2\kappa}{R}(q')^2\bar{\phi}_{\mathbf{q}}h_{\mathbf{q}'} + \left(\frac{\kappa}{R} + \frac{4T - J}{a^2} - \frac{J}{2}\mathbf{q}\cdot\mathbf{q}'\right)\bar{\phi}_{\mathbf{q}}\bar{\phi}_{\mathbf{q}'}\right\}, \tag{B16}$$

where, notably, the third line of Eq. (B15) does not contribute as it does not yield terms of second order in the perturbations. In matrix form, we find

$$F = \frac{A}{2}\sum_{\mathbf{q}\neq\mathbf{0}}(h_{\mathbf{q}} \quad \bar{\phi}_{\mathbf{q}}) \times \begin{bmatrix} \kappa q^4 + \left(\sigma - \frac{\alpha}{2}\right)q^2 & -\frac{\kappa}{R}q^2 \\ -\frac{\kappa}{R}q^2 & \frac{\kappa}{R} + \frac{4T-J}{a^2} + \frac{J}{2}q^2 \end{bmatrix}\begin{pmatrix} h_{-\mathbf{q}} \\ \bar{\phi}_{-\mathbf{q}} \end{pmatrix}. \tag{B17}$$

The matrix in Eq. (B17) is similar to the matrix $L$ in Eq. (8) of Ref. [45], which they studied to determine the flat membrane's stability. We ignore the protrusion force $f$ of Ref. [45] and set $\bar{\phi}_0 = 0$ in their $L$. Then, comparing their $L$ to the matrix in Eq. (B17), the primary difference is an overall factor $D\eta q^2/T$ that multiplies the lower row of the matrix $L$. This factor stems from $L$ being derived from a hydrodynamic equation containing the viscosity $\eta$ and a protein continuity equation containing the diffusion constant of proteins $D$; the continuity equation has two more nabla operators than the hydrodynamic equation, which explains the factor $q^2$. Importantly, this overall factor difference between the two rows of $L$ and the matrix in Eq. (B17) means that these matrices have different eigenvalues and yield different instability criteria.

## APPENDIX C: STABILITY OF AN UNCOATED CYLINDRICAL VESICLE

Here we rederive results of Refs. [18–20,71] for the stability of an uncoated cylindrical vesicle. We split Eq. (9) into $\bar{F}_H = \bar{F}_g + \bar{F}_{\bar{\sigma}} + \bar{F}_{\bar{P}}$, where

$$\bar{F}_g = \frac{1}{2}\int_0^{\bar{L}} d\bar{z}\,\frac{\bar{r}}{\sqrt{1 + (\partial_{\bar{z}}\bar{r})^2}}\left[\frac{\partial_{\bar{z}}^2\bar{r}}{1 + (\partial_{\bar{z}}\bar{r})^2} - \frac{1}{\bar{r}}\right]^2, \tag{C1a}$$

$$\bar{F}_{\bar{\sigma}} = \bar{\sigma}\int_0^{\bar{L}} d\bar{z}\,\bar{r}\sqrt{1 + (\partial_{\bar{z}}\bar{r})^2}, \tag{C1b}$$

$$\bar{F}_{\bar{P}} = \frac{1}{2}\bar{P}\int_0^{\bar{L}} d\bar{z}\,\bar{r}^2. \tag{C1c}$$

To determine the stability of a cylinder ($\bar{r} = 1$) to small perturbations ($\bar{u} \ll 1$) of its radius, we insert $\bar{r}(\bar{z}) = 1 + \bar{u}(\bar{z})$ into Eq. (C1a) [with $\bar{u}(\bar{z})$ given in Eq. (10)]. This yields

$$\bar{F}_g = \frac{1}{2}\int_0^{\bar{L}} d\bar{z}\,\frac{1 + \bar{u}}{\sqrt{1 + (\partial_{\bar{z}}\bar{u})^2}}\left[\frac{\partial_{\bar{z}}^2\bar{u}}{1 + (\partial_{\bar{z}}\bar{u})^2} - \frac{1}{1 + \bar{u}}\right]^2. \tag{C2}$$

Terms linear in $\bar{u}$ vanish for the same reason as discussed for Eq. (B4). We thus focus on terms up to $\mathcal{O}(\bar{u}^2)$. At that order, $\bar{F}_g$ reads

$$\bar{F}_g = \frac{1}{2}\int_0^{\bar{L}} d\bar{z}\,(1 + \bar{u})\left[1 - \frac{(\partial_{\bar{z}}\bar{u})^2}{2}\right]\left\{\partial_{\bar{z}}^2\bar{u}[1 - \mathcal{O}(\bar{u}^2)] - [1 - \bar{u} + \bar{u}^2 + \mathcal{O}(\bar{u}^3)]\right\}^2. \tag{C3}$$

Writing out the integrand and focusing on $\mathcal{O}(\bar{u}^2)$ terms,

$$\begin{aligned}(1 + \bar{u})&\left[1 - \frac{(\partial_{\bar{z}}\bar{u})^2}{2}\right] \times \left\{\partial_{\bar{z}}^2\bar{u}[1 - \mathcal{O}(\bar{u}^2)] - [1 - \bar{u} + \bar{u}^2 + \mathcal{O}(\bar{u}^3)]\right\}^2 \\ &= \ldots + \sum_{\bar{q},\bar{q}'\neq 0}\bar{u}_{\bar{q}}\bar{u}_{\bar{q}'}e^{i(\bar{q}+\bar{q}')\bar{z}} \times \left[2 + 1 - 2\bar{q}^2 + \bar{q}^2(\bar{q}')^2 - 2(1 - \bar{q}^2) + \frac{\bar{q}\bar{q}'}{2}\right] + \mathcal{O}(\bar{u}^3),\end{aligned} \tag{C4}$$

where we used $\partial_{\bar{z}}\bar{r} = \partial_{\bar{z}}\bar{u} = \sum_{\bar{q}\neq 0} i\bar{q}\bar{u}_{\bar{q}}e^{i\bar{q}\bar{z}}$ and $\partial_{\bar{z}}^2\bar{r} = \partial_{\bar{z}}^2\bar{u} = -\sum_{\bar{q}\neq 0}\bar{q}\bar{u}_{\bar{q}}e^{i\bar{q}\bar{z}}$. The dots represent terms linear in $\bar{u}$. We thus find

$$\bar{F}_g = \frac{\bar{L}}{2}\sum_{\bar{q}\neq 0}\bar{u}_{\bar{q}}\bar{u}_{-\bar{q}}\left(\bar{q}^4 - \frac{1}{2}\bar{q}^2 + 1\right). \tag{C5}$$

The surface tension term Eq. (C1b) reads, at $\mathcal{O}(\bar{u}^2)$,

$$\begin{aligned}\bar{F}_{\bar{\sigma}} &= \bar{\sigma}\int_0^{\bar{L}} d\bar{z}\,(1 + \bar{u})\left[1 + \frac{(\partial_{\bar{z}}\bar{u})^2}{2} + \mathcal{O}(\bar{u}^4)\right] \\ &= \frac{\bar{\sigma}\bar{L}}{2}\sum_{\bar{q}\neq 0}\bar{q}^2\bar{u}_{\bar{q}}\bar{u}_{-\bar{q}}.\end{aligned} \tag{C6}$$

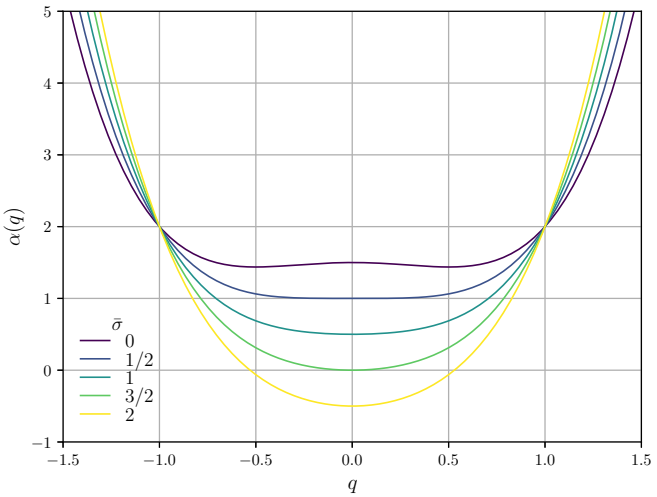


FIG. 7. Plot of $\alpha(\bar{q})$ [Eq. (C9)]. The cylindrical vesicle becomes unstable ($\alpha < 0$) for perturbations at a wavelength $\bar{q} = 0$ for $\bar{\sigma} > 3/2$.

Inserting $\bar{r}(\bar{z}) = 1 + \bar{u}(\bar{z})$ into Eq. (C1c) gives, at $\mathcal{O}(\bar{u}^2)$,

$$\bar{F}_{\bar{P}} = -\frac{\bar{P}}{2}\int_0^{\bar{L}} d\bar{z}\left(1 + \sum_{\bar{q}\neq 0}\bar{u}_{\bar{q}}e^{i\bar{q}\bar{z}}\right)^2 = -\frac{\bar{P}\bar{L}}{2}\sum_{\bar{q}\neq 0}\bar{u}_{\bar{q}}\bar{u}_{-\bar{q}}. \tag{C7}$$

Collecting Eqs. (C5)–(C7) now yields

$$\bar{F}_H = \frac{\bar{L}}{4}\sum_{\bar{q}\neq 0}\bar{u}_{\bar{q}}\bar{u}_{-\bar{q}}[2\bar{q}^4 + \bar{q}^2(2\bar{\sigma} - 1) + 2 - 2\bar{P}]. \tag{C8}$$

Inserting the Laplace pressure $\bar{P} = \bar{\sigma} - 1/2$ [the first terms of Eq. (5)] into Eq. (C8) gives [18–20,71]

$$\bar{F}_H = \frac{\bar{L}}{2}\sum_{\bar{q}\neq 0}\bar{u}_{\bar{q}}\bar{u}_{-\bar{q}}\underbrace{\bar{\sigma}(\bar{q}^2 - 1) + \bar{q}^4 - \frac{1}{2}\bar{q}^2 + \frac{3}{2}}_{\alpha(\bar{q})}; \tag{C9}$$

$\alpha(\bar{q})$ has minima when $\partial_{\bar{q}}\alpha(\bar{q}) = \bar{q}(4\bar{q}^2 + 2\bar{\sigma} - 1) = 0$, which happens at $\bar{q} = 0$ and $\bar{q} = \pm\frac{1}{2}\sqrt{1 - 2\bar{\sigma}}$, see also Fig. 7, where we plot $\alpha(q)$. The cylinder is stable if $\alpha(q = 0) = -\bar{\sigma} + 3/2 > 0$; hence $\bar{\sigma} < 3/2$. In terms of the original variables, this reads $\sigma R^2/\kappa < 3/2$; hence $R < \sqrt{3\kappa/(2\sigma)}$.

## APPENDIX D: STABILITY OF A COATED CYLINDRICAL VESICLE [DERIVATION OF EQ. (11)]

Of the free energy $\bar{F} = \bar{F}_H + \bar{F}_\phi$ [Eq. (9)] of a cylindrical vesicle coated with proteins, we considered the membrane instabilities associated with $\bar{F}_H$ in Section C. Next, we partition $\bar{F}_\phi$ into $\bar{F}_\phi = \bar{F}_{\bar{\Lambda}} + \bar{F}_{\bar{\mu}} + \bar{F}_{\bar{a}} + \bar{F}_{\bar{b}}$, where

$$\bar{F}_{\bar{\Lambda}} = -\frac{\bar{\Lambda}}{2}\int_0^{\bar{L}} d\bar{z}\,\bar{\phi}\left[\frac{\bar{r}\partial_{\bar{z}}^2\bar{r}}{1 + (\partial_{\bar{z}}\bar{r})^2} - 1\right], \tag{D1a}$$

$$\bar{F}_{\bar{\mu}} = -\bar{\mu}\int_0^{\bar{L}} d\bar{z}\,\bar{r}\sqrt{1 + (\partial_{\bar{z}}\bar{r})^2}\bar{\phi}, \tag{D1b}$$

$$\bar{F}_{\bar{a}} = \frac{\bar{a}}{2}\int_0^{\bar{L}} d\bar{z}\,\bar{r}\sqrt{1 + (\partial_{\bar{z}}\bar{r})^2}\bar{\phi}^2, \tag{D1c}$$

$$\bar{F}_{\bar{b}} = \frac{\bar{b}}{2}\int_0^{\bar{L}} d\bar{z}\,\bar{r}\sqrt{1 + (\partial_{\bar{z}}\bar{r})^2}(\partial_{\bar{z}}\bar{\phi})^2. \tag{D1d}$$

We insert $\bar{r}(\bar{z}) = 1 + \bar{u}(\bar{z})$ and $\bar{\phi} = 1 + \bar{\varphi}(\bar{z})$ [with $\bar{u}(\bar{z})$ and $\bar{\varphi}(\bar{z})$ as in Eq. (10)] in each of these terms. Again, constant terms cannot affect any physical observable, and terms linear in the perturbations drop for the reason shown in Eq. (B4). At quadratic order, we find

$$\bar{F}_{\bar{\Lambda}} = \frac{\bar{L}\bar{\Lambda}}{2}\sum_{\bar{q}\neq 0}\bar{q}^2(\bar{u}_{\bar{q}}\bar{u}_{-\bar{q}} + \bar{\phi}_{\bar{q}}\bar{u}_{-\bar{q}}), \tag{D2a}$$

$$\bar{F}_{\bar{\mu}} = -\frac{\bar{L}\bar{\mu}}{2}\sum_{\bar{q}\neq 0}2\bar{\phi}_{\bar{q}}\bar{u}_{-\bar{q}} + \bar{u}_{\bar{q}}\bar{u}_{-\bar{q}}\bar{q}^2, \tag{D2b}$$

$$\bar{F}_{\bar{a}} = \frac{\bar{L}\bar{a}}{2}\sum_{\bar{q}\neq 0}2\bar{\phi}_{\bar{q}}\bar{u}_{-\bar{q}} + \bar{u}_{\bar{q}}\bar{u}_{-\bar{q}}\frac{\bar{q}^2}{2} + \bar{\phi}_{\bar{q}}\bar{\phi}_{-\bar{q}}, \tag{D2c}$$

$$\bar{F}_{\bar{b}} = \frac{\bar{L}\bar{b}}{2}\sum_{\bar{q}\neq 0}\bar{q}^2\bar{\phi}_{\bar{q}}\bar{\phi}_{-\bar{q}}. \tag{D2d}$$

Gathering Eqs. (D2a)–(D2d) yields

$$\bar{F}_\phi = \frac{\bar{L}}{4}\sum_{\bar{q}\neq 0}[\bar{q}^2(\bar{\Lambda} - \bar{a})\bar{u}_{\bar{q}}\bar{u}_{-\bar{q}} + 2\bar{\Lambda}(\bar{q}^2 - 1)\bar{u}_{\bar{q}}\bar{\phi}_{-\bar{q}} + 2(\bar{a} + \bar{b}\bar{q}^2)\bar{\phi}_{\bar{q}}\bar{\phi}_{-\bar{q}}]. \tag{D3}$$

where we used $\bar{\mu} = \bar{a} + \bar{\Lambda}/2$ [Eq. (4), nondimensionalized]. Combining Eqs. (C8) and (D3) yields Eq. (11).

## APPENDIX E: FLAT-MEMBRANE LIMIT OF EQ. (11)

We write out Eq. (11) and return to dimensional units

$$F = \frac{\pi L}{2R}\sum_{q\neq 0}\begin{pmatrix}u_q & \phi_q\end{pmatrix}\begin{bmatrix}2\kappa q^4R^2 + (\Lambda\Phi R - a\Phi^2R^2 + 2\sigma R^2 - \kappa)q^2 + \frac{\Lambda\Phi}{R} + a\Phi^2 - 2\sigma + \frac{3\kappa}{R^2} & \Lambda(q^2R^2 - 1)\\ \Lambda(q^2R^2 - 1) & 2aR^2 + 2bq^2R^2\end{bmatrix}\begin{pmatrix}u_{-q}\\ \phi_{-q}\end{pmatrix}. \tag{E1}$$

We now find that the leading-order term in the limit of a large radius $R$ reads

$$F = \frac{2\pi RL}{2}\sum_{q\neq 0}\begin{pmatrix}u_q & \phi_q\end{pmatrix}\begin{bmatrix}\kappa q^4 + (\sigma - a\Phi^2/2)q^2 & \frac{1}{2}\Lambda q^2\\ \frac{1}{2}\Lambda q^2 & a + bq^2\end{bmatrix}\begin{pmatrix}u_{-q}\\ \phi_{-q}\end{pmatrix} + \mathcal{O}(1). \tag{E2}$$

The prefactor $2\pi RL$ being the area of the (large-radius) cylinder, we recognize that the above expression is the same free energy per unit area as Eq. (B7).

## APPENDIX F: LINEARIZED EQUATIONS FOR AN AXISYMMETRIC MEMBRANE TUBE

We assume a ground state with no flow and membrane given by the vector $\mathbf{X}(\theta, z) = [(R + \epsilon u(z))\cos\theta, (R + \epsilon u(z))\sin\theta, z]$, and protein distribution $\phi = \Phi + \epsilon\delta\phi(z)$ where $\epsilon \ll 1$. Moreover, we assume all flows are of order $\epsilon$. We assume the surface tension and chemical potential to be of the form $\sigma(z) = \sigma_0 + \epsilon\delta\sigma(z)$ and $\mu(z) = \mu_0 + \epsilon\chi\delta\phi$ where $\chi$ is the proteins' 2D inverse compressibility. These assumptions give the following linearized equations for an axisymmetric membrane tube. First, the shape operator amounts to

$$\mathbf{S} = -\nabla\mathbf{N} = -\frac{R - \epsilon u}{R^2}\mathbf{e}_\theta\mathbf{e}_\theta + \epsilon\partial_{zz}u\mathbf{e}_z\mathbf{e}_z, \tag{F1}$$

giving the following mean and Gaussian curvatures:

$$H = -\frac{1}{2R} + \epsilon\frac{\partial_{zz}u}{2} + \epsilon\frac{u}{2R^2}, \tag{F2a}$$

$$K = -\frac{\epsilon\partial_{zz}u}{R}. \tag{F2b}$$

Second, surface incompressibility [Eq. (22)] gives, at first order,

$$\partial_z v^z + \frac{1}{R}\dot{u} = 0. \tag{F3}$$

Third, using Eq. (23), tangential force balance is given by

$$\partial_z\delta\sigma + 2\eta_m\partial_z^2 v^z - \chi\Phi\partial_z\delta\phi = \eta\vec{e}_z\cdot[\mathcal{D}]\cdot\vec{e}_r, \tag{F4}$$

and normal force balance on the membrane is given by

$$-\left\{\kappa\epsilon\left(\partial_z^4 u + \frac{1}{2R^2}\partial_z^2 u + \frac{3}{2R^4}u\right) - \frac{\kappa}{2R^3} - \frac{\epsilon\Lambda}{2}\partial_z^2\delta\phi - \epsilon\frac{\Lambda\Phi}{R}\partial_z^2 u + \frac{a\Phi^2}{2R} + \epsilon\frac{a\Phi}{R}\delta\phi - \epsilon a\Phi^2\left(\frac{u}{2R^2} + \frac{\partial_z^2 u}{2}\right)\right\}$$
$$-\frac{\sigma_0}{R} + \epsilon\sigma_0\left(\partial_z^2 u + \frac{u}{R^2}\right) - \epsilon\frac{\delta\sigma}{R} + \frac{\mu_0\Phi}{R} + \epsilon\left[\frac{\mu_0\delta\phi}{R} + \frac{\chi\Phi\delta\phi}{R} - \mu_0\Phi\left(\partial_z^2 u + \frac{u}{R^2}\right)\right] - 2\frac{\eta_m}{R^2}\dot{u} = \eta\vec{e}_r\cdot[\mathcal{D}]\cdot\vec{e}_r - [P]. \tag{F5}$$

Fourth, the protein dynamics [Eq. (24)] is governed by

$$\partial_t\delta\phi - aM\partial_z^2\delta\phi + \frac{\Lambda M}{2}\left(\partial_z^4 u + \frac{1}{R^2}\partial_z^2 u\right) + bM\partial_z^4\delta\phi = 0. \tag{F6}$$

The solutions to the Stokes equation [Eq. (21a)] in cylindrical coordinates $(r, \theta, z)$ inside $(-)$ and outside $(+)$ the tube are given by [76]

$$\vec{V}^\pm = \vec{\nabla}\zeta^\pm + \vec{\nabla}\times\left(\psi^\pm\vec{e}_z\right) + r\partial_r\vec{\nabla}\xi^\pm + \partial_z\xi^\pm\vec{e}_z, \tag{F7a}$$

$$P^\pm = -2\eta\partial_z^2\xi^\pm + P_0^\pm, \tag{F7b}$$

$$(\zeta^\pm, \psi^\pm, \xi^\pm)^T = \int\frac{dq}{2\pi}(Z^\pm, \Psi^\pm, \Xi^\pm)^T\Pi_q^\pm(r)e^{iqz}, \tag{F7c}$$

$$\text{where}\quad \Pi_q^\pm(r) = \begin{cases}\Pi_q^+(r) = K_0(qr),\\ \Pi_q^-(r) = I_0(qr).\end{cases}$$

Taking the Fourier transform in $z$ [$f(z) = \int dq\bar{f}_q e^{iqz}/(2\pi)$, $\mathcal{F}_q[f(z)] = \bar{f}(q)$] of the linear perturbations in Eqs. (F3)–(F5) yields

$$iq\bar{v}_q^z + \frac{1}{R}\partial_t\bar{u}_q = 0, \tag{F8}$$

$$iq\delta\bar{\sigma}_q - 2q^2\eta_m\bar{v}_q^z - iq\chi\Phi\delta\bar{\phi}_q = \mathcal{F}_q\{\eta\vec{e}_z\cdot[\mathcal{D}]\cdot\vec{e}_r\}, \tag{F9}$$

$$\partial_t\delta\bar{\phi}_q = -(bMq^4 + aMq^2)\delta\bar{\phi}_q + \frac{\Lambda M}{2}\bar{u}_q\left(\frac{q^2}{R^2} - q^4\right). \tag{F10}$$

Similarly, Fourier transforming Eq. (F6) gives

$$-\left\{\kappa\left[\epsilon\left(q^4 - \frac{1}{2R^2}q^2 + \frac{3}{2R^4}\right)\bar{u}_q - \frac{1}{2R^3}\delta(q)\right] + \frac{\epsilon\Lambda}{2}q^2\delta\bar{\phi}_q + \epsilon\frac{\Lambda\Phi}{R}q^2\bar{u}_q + \frac{a\Phi^2}{2R}\delta(q) + \epsilon\frac{a\Phi}{R}\delta\bar{\phi}_q - \epsilon a\Phi^2\bar{u}_q\left(\frac{1}{2R^2} - \frac{q^2}{2}\right)\right\}$$
$$-\frac{\sigma_0}{R}\delta(q) + \epsilon\sigma_0\bar{u}_q\left(\frac{1}{R^2} - q^2\right) - \epsilon\frac{\delta\bar{\sigma}_q}{R} + \frac{\mu_0\Phi}{R}\delta(q) + \epsilon\left[\frac{\mu_0\delta\bar{\phi}_q}{R} + \frac{\chi\Phi\delta\bar{\phi}_q}{R} - \mu_0\Phi\bar{u}_q\left(\frac{1}{R^2} - q^2\right)\right] - 2\frac{\eta_m}{R^2}\partial_t\bar{u}_q$$
$$= \mathcal{F}_q\{\eta\vec{e}_r\cdot[\mathcal{D}]\cdot\vec{e}_r - [P]\}. \tag{F11}$$

For the unperturbed state ($\epsilon = 0$), Eqs. (F10) and (F11) are solved for the ground state conditions found via the free-energy analysis, Eqs. (4) and (5).

We solve the ambient Stokes equations [Eq. (21)] in Fourier space for no-slip boundary conditions ($\vec{V}|_R = \mathbf{V}$). We have $\Psi^{\pm} = 0$ as the system is axisymmetric. The other coefficients amount to

$$Z^+ = \frac{K_1(qR)(qR\partial_t\bar{u}_q - i\bar{v}_q^z) - K_0(qR)(\partial_t\bar{u}_q + iqR\bar{v}_q^z)}{q[qRK_0(qR)^2 + 2K_1(qR)K_0(qR) - qRK_1(qR)^2]}, \tag{F12a}$$

$$Z^- = \frac{I_1(qR)(-qR\partial_t\bar{u}_q + i\bar{v}_q^z) - I_0(qR)(\partial_t\bar{u}_q + iqR\bar{v}_q^z)}{q[qRI_0(qR)^2 - 2I_1(qR)I_0(qR) - qRI_1(qR)^2]}, \tag{F12b}$$

$$\Xi^+ = \frac{\partial_t\bar{u}_q K_0(qR) - i\bar{v}_q^z K_1(qR)}{q[qRK_0(qR)^2 + 2K_1(qR)K_0(qR) - qRK_1(qR)^2]}, \tag{F12c}$$

$$\Xi^- = \frac{\partial_t\bar{u}_q I_0(qR) + i\bar{v}_q^z I_1(qR)}{q[qRI_0(qR)^2 - 2I_1(qR)I_0(qR) - qRI_1(qR)^2]}. \tag{F12d}$$

The ambient velocities and pressures in Fourier space are then given by

$$\bar{V}_q^+ = \left\{q^2 r\Xi^+\left[K_0(qr) + \frac{K_1(qr)}{qr}\right] - qZ^+K_1(qr)\right\}\vec{e}_r + \left\{iqr\Xi^+\left[\frac{K_0(qr)}{r} - qK_1(qr)\right] + iqZ^+K_0(qr)\right\}\vec{e}_z, \tag{F13a}$$

$$\bar{V}_q^- = \left\{q^2 r\Xi^-\left[I_0(qr) - \frac{I_1(qr)}{qr}\right] + qZ^-I_1(qr)\right\}\vec{e}_r + \left\{iqr\Xi^-\left[\frac{I_0(qr)}{r} + qI_1(qr)\right] + iqZ^-I_0(qr)\right\}\vec{e}_z, \tag{F13b}$$

$$\bar{P}^+ = P_0^+ + 2\eta q^2\Xi^+K_0(qr), \tag{F13c}$$

$$\bar{P}^- = P_0^- + 2\eta q^2\Xi^-I_0(qr). \tag{F13d}$$

The tangential force balance and continuity equations [Eqs. (F8) and (F9)] can be solved for the surface tension variation, giving

$$\delta\bar{\sigma}_q = \delta\bar{\phi}_q\Phi\chi + \frac{2\eta_m\partial_t\bar{u}_q}{R} + \frac{2\eta\partial_t\bar{u}_q\{qRI_0(qR)[qRK_0(qR) + K_1(qR)] - I_1(qR)[(q^2R^2+2)K_1(qR) + qRK_0(qR)]\}}{q^2R^2[qRI_0(qR)^2 - 2I_1(qR)I_0(qR) - qRI_1(qR)^2][qRK_0(qR)^2 + 2K_1(qR)K_0(qR) - qRK_1(qR)^2]}. \tag{F14}$$

Substituting Eq. (F14) into the shape equation, Eq. (F11), we find

$$-\frac{\kappa}{2R^4}(2\bar{q}^4 + \zeta_2\bar{q}^2 + \zeta_0)\bar{u}_q - \frac{\Lambda}{2R^3}(\bar{q}^2 - 1)\delta\bar{\phi}_q = \frac{2\eta}{R^2}\left(\beta + 2\frac{\eta_m}{R\eta}\right)\partial_t\bar{u}_q, \tag{F15}$$

where $\zeta_2$ and $\zeta_0$ were defined below Eq. (11) and $\beta$ in Eq. (25c). With nondimensionalization with respect to the timescale $\eta R/\kappa$, lengthscale $R$, and concentration $\Phi$, we find that Eqs. (F10) and (F15) and reduce to Eq. (25a).

## APPENDIX G: ENERGY-MINIMIZING SHAPES

To determine the energy-minimizing shapes, we write Eqs. (1) and (2) in dimensionless variables,

$$2\pi\bar{F} = \int d\bar{A}\left\{2[\bar{H} - \bar{C}(\bar{\phi})]^2 + \widetilde{\sigma}(\bar{\phi}) + R^2\frac{\bar{b}}{2}|\nabla\bar{\phi}|^2\right\} - \bar{P}\int d\bar{V}, \tag{G1}$$

with $d\bar{A} = R^{-2}\,dA$, $d\bar{V} = R^{-3}\,dV$, $\bar{H} = RH$, $\bar{C}(\bar{\phi}) = \bar{\Lambda}\bar{\phi}/4$, and $\widetilde{\sigma}(\bar{\phi}) = \bar{\sigma} - (\bar{a} + \bar{\Lambda}/2)\bar{\phi} + (\bar{a}/2 - \bar{\Lambda}/8)\bar{\phi}^2$. The term $R^2\bar{b}|\nabla\bar{\phi}|^2/2$ acts as a line tension between dilute and dense protein domains. To estimate the magnitude of the line tension, we consider a cylindrical tube with dimensionless radius $\bar{r}_b$. The protein density changes over a dimensionless length $\bar{l}$ from a dense domain with density $\bar{\phi}^{(\mathrm{I})}$ to a dilute domain, with density $\bar{\phi}^{(\mathrm{II})}$. If the mean curvature follows the spontaneous curvature, $\bar{H} = \bar{C}$, the contribution of the domain boundary to the free energy, which we denote as $\bar{F}_b$, is approximated by

$$2\pi\bar{F}_b = 2\pi\bar{r}_b\bar{l}\left\{\bar{\sigma} + \frac{\bar{b}}{2}\left[\frac{\bar{\phi}^{(\mathrm{I})} - \bar{\phi}^{(\mathrm{II})}}{\bar{l}}\right]^2\right\}, \tag{G2}$$

where we use $\widetilde{\sigma} \approx \bar{\sigma}$. Minimizing $\bar{F}_b$ with respect to $\bar{l}$ and reinserting $\bar{l}$ into Eq. (G2) leads to $2\pi\bar{F}_b = 2\pi\bar{r}_b\gamma$, with $\gamma = \sqrt{2\bar{b}\bar{\sigma}}[\bar{\phi}^{(\mathrm{I})} - \bar{\phi}^{(\mathrm{II})}]$. The free energy of the coated membrane tube is now written as $2\pi\bar{F}_b = \widetilde{F} + 2\pi\bar{r}_b\gamma$, with $\widetilde{F} = \int d\bar{A}\{[\bar{H} - \bar{C}(\bar{\phi})]^2 + \widetilde{\sigma}(\bar{\phi})\} - \bar{P}\int d\bar{V}$. Within a domain with constant $\bar{\phi}$, the functional variation of $\widetilde{F}$ leads to the following shape equation [12]:

$$\frac{\bar{P}}{2} = \nabla^2\bar{H} + 2[\bar{H} - \bar{C}(\bar{\phi})][\bar{H}^2 + \bar{H}\bar{C}(\bar{\phi}) - \bar{K}] - \widetilde{\sigma}(\bar{\phi})\bar{H}. \tag{G3}$$

Although only the mean curvature $\bar{H}$ enters into the energy functional $\widetilde{F}$, the Gaussian curvature $\bar{K}$, here in units of $R^{-2}$, appears in the shape equation [12]. A shape with constant mean curvature, a so-called Delaunay shape [75], solves Eq. (G3) if

$$\bar{P} = -2\widetilde{\sigma}(\bar{\phi})\bar{H}, \tag{G4a}$$

$$[\bar{H} - \bar{C}(\bar{\phi})][\bar{H}^2 + \bar{H}\bar{C}(\bar{\phi}) - \bar{K}] = 0. \tag{G4b}$$

Below we discuss solutions of Eq. (G3) for different $\bar{\Lambda}$.

#### 1. $\bar{\Lambda} < 0$; one continuous protein domain

The protein density $\bar{\phi}$ sets the spontaneous curvature $\bar{C}$. To fulfill the conditions in Eq. (G4), the mean curvature has to equal the spontaneous curvature, $\bar{H} = \bar{C}(\bar{\phi})$. To fully describe the shape, we must specify the mean curvature and the minimum radius $\bar{r}_{\min}$. For a given $\bar{\phi}$, $\bar{r}_{\min}$ is varied so that the volume of the undulating shape is equal to the volume of a cylinder of the same length and with radius $\bar{r} = 1$. Subsequently, $\bar{\phi}$ is varied to determine the shape with minimal energy. For $\bar{\Lambda} = -1.8$, we find $\bar{\phi} = 1.112$, $\bar{H} = -0.5004$, and $\bar{r}_{\min} = 0.96$.

#### 2. $\bar{\Lambda} > 0$; one continuous protein domain

In analogy to the case for negative $\bar{\Lambda}$, we find that a solution to the shape equation has to fulfill $\bar{H} = \bar{C}(\bar{\phi})$ and thus $\bar{H} = \bar{\Lambda}\bar{\phi}/4$. Since both $\bar{\Lambda}$ and $\bar{\phi}$ are positive, $\bar{H}$ has to be positive as well. There are no cylindrically symmetric, non-self-intersecting shapes with $\bar{H} > 0$. Hence, there is no physically meaningful solution to Eq. (G3).

#### 3. $\bar{\Lambda} < 0$; alternating dense and dilute domains

The protein densities $\bar{\phi}^{(\mathrm{I})}$ (dense) and $\bar{\phi}^{(\mathrm{II})}$ (dilute) set a spontaneous curvature in the respective domain. Condition Eq. (G4b) is fulfilled if the mean curvatures in each domain equal the spontaneous curvature. Furthermore, according to condition Eq. (G4a), the two densities are linked via $\widetilde{\sigma}[\bar{\phi}^{(\mathrm{I})}]\bar{C}[\bar{\phi}^{(\mathrm{I})}] = \widetilde{\sigma}[\bar{\phi}^{(\mathrm{II})}]\bar{C}[\bar{\phi}^{(\mathrm{II})}]$, since the pressure does not vary along the tube. For a given $\bar{\phi}^{(\mathrm{I})}$, the corresponding $\bar{\phi}^{(\mathrm{II})}$ and thus mean curvatures in the two domains are set. To fully describe the tube shape, we need to find the minimal tube radius $\bar{r}_{\min}$ and the radius at the boundary of the dense and dilute domain $\bar{r}_b$. To determine the two parameters, we start by setting $\bar{\phi}^{(\mathrm{I})}$ and $\bar{r}_{\min}$ to fixed values and adjust $\bar{r}_b$ such that volume conservation is achieved. Subsequently, we vary $\bar{\phi}^{(\mathrm{I})}$ and $\bar{r}_{\min}$ to find the shape with the lowest energy. For $\bar{\Lambda} = -1.8$, we find $\bar{\phi}^{(\mathrm{I})} = 2.763$, which corresponds to $\bar{\phi}^{(\mathrm{II})} = 0$, $\bar{H}^{(\mathrm{I})} = -1.243$, $\bar{H}^{(\mathrm{II})} = 0$ and $\bar{r}_{\min} = 0.7$, $\bar{r}_b = 1.322$.

#### 4. $\bar{\Lambda} > 0$; alternating dense and dilute domains

We again note that the protein densities set the spontaneous curvature in the dense and dilute domains. However, as discussed under in Section G 2, a physically meaningful shape cannot have a positive mean curvature everywhere. Instead, a feasible solution must exhibit alternations between positive and negative mean curvature domains. We note that, for $\bar{C} = 0$, i.e., in a protein-free domain, condition Eq. (G4b) is fulfilled if the square of the mean curvature and the Gaussian curvature are identical. Or, equivalently, the two principle curvatures have to be identical. A shape with two identical, negative principle curvatures corresponds to a segment of a sphere. Based on these notions, we look for a shape that alternates between a protein-free domain $\bar{\phi}^{(\mathrm{II})} = 0$, with a negative mean curvature $\bar{H}^{(\mathrm{II})}$ that follows a spherical shape and a protein-coated domain $\bar{\phi}^{(\mathrm{I})}$, where the mean curvature follows the spontaneous curvature, $\bar{H}^{(\mathrm{II})} = \bar{C}[\bar{\phi}^{(\mathrm{I})}]$. The protein density $\bar{\phi}^{(\mathrm{I})}$ is set by Eq. (G4a), which amounts to $\widetilde{\sigma}[\bar{\phi}^{(\mathrm{I})}]\bar{C}[\bar{\phi}^{(\mathrm{I})}] = \widetilde{\sigma}(0)\bar{H}^{(\mathrm{II})}$. To fully describe the tube shape, we need to find the minimal tube radius $\bar{r}_{\min}$ and the radius at the boundary of the dense and dilute domain $\bar{r}_b$. We follow a similar procedure as described in Section G 3. For a fixed $\bar{r}_{\min}$, $\bar{r}_b$ is adjusted to ensure volume conservation. Subsequently, $\bar{r}_{\min}$ is varied to find the energy-minimizing shape. For $\bar{\Lambda} = 1.8$, we find $\bar{\phi}^{(\mathrm{I})} = 1.002$, and $\bar{r}_{\min} = 0.291$, $\bar{r}_b = 0.29$, which implies $\bar{H}^{(\mathrm{I})} = 0.451$ and $\bar{H}^{(\mathrm{II})} = -0.772$.


[1] U. Seifert, Adv. Phys. **46**, 13 (1997).

[2] I. Derényi, F. Jülicher, and J. Prost, Phys. Rev. Lett. **88**, 238101 (2002).

[3] T. R. Powers, G. Huber, and R. E. Goldstein, Phys. Rev. E **65**, 041901 (2002).

[4] A. Yamada, A. Mamane, J. Lee-Tin-Wah, A. Di Cicco, C. Prévost, D. Lévy, J.-F. Joanny, and P. Coudrier, Evelyne Bassereau, Nat. Commun. **5**, 3624 (2014).

[5] M. Drab, D. Stopar, V. Kralj-Iglič, and A. Iglič, Cells **8**, 626 (2019).

[6] J. Hurtig, D. T. Chiu, and B. Önfelt, WIREs Nanomed. Nanobiotechnol. **2**, 260 (2010).

[7] J. Nixon-Abell, C. J. Obara, A. V. Weigel, D. Li, W. R. Legant, C. S. Xu, H. A. Pasolli, K. Harvey, H. F. Hess, E. Betzig, C. Blackstone, and J. Lippincott-Schwartz, Science **354**, aaf3928 (2016).

[8] J. F. Presley, N. B. Cole, T. A. Schroer, K. Hirschberg, K. J. M. Zaal, and J. Lippincott-Schwartz, Nature (Lond.) **389**, 81 (1997).

[9] P. Bassereau, R. Jin, T. Baumgart, M. Deserno, R. Dimova, V. A. Frolov, P. V. Bashkirov, H. Grubmüller, R. Jahn, H. J. Risselada, L. Johannes, M. M. Kozlov, R. Lipowsky, T. J. Pucadyil, W. F. Zeno, J. C. Stachowiak, D. Stamou, A. Breuer, L. Lauritsen, C. Simon *et al.*, J. Phys. D **51**, 343001 (2018).

[10] W. Helfrich, Zeitschr. Naturforsch. C **28**, 693 (1973).

[11] T. R. Powers, Rev. Mod. Phys. **82**, 1607 (2010).

[12] M. Deserno, Chem. Phys. Lipids **185**, 11 (2015).

[13] J. Guven and P. Vázquez-Montejo, in *The Role of Mechanics in the Study of Lipid Bilayers* (Springer, Berlin, 2018), pp. 167–219.

[14] O.-Y. Zhong-Can and W. Helfrich, Phys. Rev. A **39**, 5280 (1989).

[15] S. Chaïeb and S. Rica, Phys. Rev. E **58**, 7733 (1998).
[16] R. Bar-Ziv and E. Moses, Phys. Rev. Lett. **73**, 1392 (1994).
[17] D. J. Bukman, J. H. Yao, and M. Wortis, Phys. Rev. E **54**, 5463 (1996).
[18] K. Gurin, V. Lebedev, and A. Muratov, Zh. Éksp. Teor. Fiz. **110**, 600 (1996) [Sov. Phys. JETP **83**, 321 (1996)].
[19] R. E. Goldstein, P. Nelson, T. Powers, and U. Seifert, J. Phys. II **6**, 767 (1996).
[20] S. C. Al-Izzi, G. Rowlands, P. Sens, and M. S. Turner, Phys. Rev. Lett. **120**, 138102 (2018).
[21] V. Markin, Biophys. J. **36**, 1 (1981).
[22] S. Leibler and D. Andelman, J. Phys. France **48**, 2013 (1987).
[23] T. Kawakatsu, D. Andelman, K. Kawasaki, and T. Taniguchi, J. Phys. II **3**, 971 (1993).
[24] T. Taniguchi, K. Kawasaki, D. Andelman, and T. Kawakatsu, J. Phys. II **4**, 1333 (1994).
[25] T. Taniguchi, Phys. Rev. Lett. **76**, 4444 (1996).
[26] P. B. Sunil Kumar and M. Rao, Phys. Rev. Lett. **80**, 2489 (1998).
[27] S. Givli, H. Giang, and K. Bhattacharya, SIAM J. Appl. Math. **72**, 489 (2012).
[28] S. Katz and S. Givli, Comput. Math. Methods Med. **2017**, 1 (2017).
[29] A. Sahu, R. A. Sauer, and K. K. Mandadapu, Phys. Rev. E **96**, 042409 (2017).
[30] P. Nowakowski, B. H. Stumpf, A.-S. Smith, and A. Maciołek, arXiv:2206.03424 (2022).
[31] V. Frette, I. Tsafrir, M.-A. Guedeau-Boudeville, L. Jullien, D. Kandel, and J. Stavans, Phys. Rev. Lett. **83**, 2465 (1999).
[32] M. Breidenich, R. Netz, and R. Lipowsky, Europhys. Lett. **49**, 431 (2000).
[33] I. Tsafrir, D. Sagi, T. Arzi, M.-A. Guedeau-Boudeville, V. Frette, D. Kandel, and J. Stavans, Phys. Rev. Lett. **86**, 1138 (2001).
[34] F. Campelo and A. Hernandez-Machado, Eur. Phys. J.: Spec. Top. **143**, 101 (2007).
[35] F. Campelo and A. Hernández-Machado, Phys. Rev. Lett. **99**, 088101 (2007).
[36] R. R. Netz and P. Pincus, Phys. Rev. E **52**, 4114 (1995).
[37] R. Lipowsky and H.-G. Döbereiner, Europhys. Lett. **43**, 219 (1998).
[38] H. Noguchi and M. Takasu, Biophys. J. **83**, 299 (2002).
[39] M. Deserno, Phys. Rev. E **69**, 031903 (2004).
[40] I. Palaia, A. Paraschiv, V. E. Debets, C. Storm, and A. Šarić, ACS Nano **15**, 15794 (2021).
[41] D. Andelman, M. Kozlov, and W. Helfrich, Europhys. Lett. **25**, 231 (1994).
[42] S. Ramaswamy, J. Toner, and J. Prost, Phys. Rev. Lett. **84**, 3494 (2000).
[43] R. Shlomovitz and N. Gov, Phys. Biol. **6**, 046017 (2009).
[44] R. Shlomovitz, N. Gov, and A. Roux, New J. Phys. **13**, 065008 (2011).
[45] A. Veksler and N. S. Gov, Biophys. J. **93**, 3798 (2007).
[46] T. Auth and G. Gompper, Phys. Rev. E **80**, 031901 (2009).
[47] D. Kabaso, N. Bobrovska, W. Góźdź, N. Gov, V. Kralj-Iglič, P. Veranič, and A. Iglič, J. Biomech. **45**, 231 (2012).
[48] N. Gov, Philos. Trans. Roy. Soc. B: Biol. Sci. **373**, 20170115 (2018).
[49] C. Tozzi, N. Walani, and M. Arroyo, New J. Phys. **21**, 093004 (2019).
[50] M. Fošnarič, S. Penič, A. Iglič, V. Kralj-Iglič, M. Drab, and N. S. Gov, Soft Matter **15**, 5319 (2019).
[51] S. Leibler, J. Phys. **47**, 507 (1986).
[52] J. Derganc, Phys. Biol. **4**, 317 (2007).
[53] H. Noguchi, Soft Matter **17**, 10469 (2021).
[54] J. C. Stachowiak, E. M. Schmid, C. J. Ryan, H. S. Ann, D. Y. Sasaki, M. B. Sherman, P. L. Geissler, D. A. Fletcher, and C. C. Hayden, Nat. Cell Biol. **14**, 944 (2012).
[55] M. Lindén, P. Sens, and R. Phillips, PLoS Comput. Biol. **8**, e1002431 (2012).
[56] S. Liese, E. M. Wenzel, I. Kjos, R. R. Molina, S. W. Schultz, A. Brech, H. Stenmark, C. Raiborg, and A. Carlson, Proc. Natl. Acad. Sci. USA **117**, 28614 (2020).
[57] S. Liese and A. Carlson, Biophys. J. **120**, 2482 (2021).
[58] F. Yuan, H. Alimohamadi, B. Bakka, A. N. Trementozzi, K. J. Day, N. L. Fawzi, P. Rangamani, and J. C. Stachowiak, Proc. Natl. Acad. Sci. USA **118**, e2017435118 (2021).
[59] J. Zimmerberg and M. M. Kozlov, Nat. Rev. Mol. Cell Biol. **7**, 9 (2006).
[60] M. Schulz, A. Olubummo, and W. H. Binder, Soft Matter **8**, 4849 (2012).
[61] H. Alimohamadi and P. Rangamani, Biomolecules **8**, 120 (2018).
[62] R. Capovilla and J. Guven, J. Phys.: Condens. Matter **16**, S2187 (2004).
[63] J. Klebes, P. Clegg, and R. M. L. Evans, Phys. Rev. E **105**, 064802 (2022).
[64] A. Callan-Jones and P. Bassereau, Curr. Opin. Solid State Mater. Sci. **17**, 143 (2013).
[65] M. Naoz and N. S. Gov, Cells **9**, 782 (2020).
[66] D. Gonzalez-Rodriguez, S. Sart, A. Babataheri, D. Tareste, A. I. Barakat, C. Clanet, and J. Husson, Phys. Rev. Lett. **115**, 088102 (2015).
[67] N. Patil, S. Bonneau, F. Joubert, A.-F. Bitbol, and H. Berthoumieux, Phys. Rev. E **102**, 022401 (2020).
[68] S. A. Rautu, D. Orsi, L. Di Michele, G. Rowlands, P. Cicuta, and M. S. Turner, Soft Matter **13**, 3480 (2017).
[69] C. Morris and U. Homann, J. Membr. Biol. **179**, 79 (2001).
[70] F. Jülicher and R. Lipowsky, Phys. Rev. E **53**, 2670 (1996).
[71] J. Tchoufag, A. Sahu, and K. K. Mandadapu, Phys. Rev. Lett. **128**, 068101 (2022).
[72] A. R. Honerkamp-Smith, F. G. Woodhouse, V. Kantsler, and R. E. Goldstein, Phys. Rev. Lett. **111**, 038103 (2013).
[73] F. Quemeneur, J. K. Sigurdsson, M. Renner, P. J. Atzberger, P. Bassereau, and D. Lacoste, Proc. Natl. Acad. Sci. USA **111**, 5083 (2014).
[74] V. Narsimhan, A. P. Spann, and E. S. G. Shaqfeh, J. Fluid Mech. **777**, 1 (2015).
[75] C. Delaunay, J. Math. Pures Appl. **6**, 309 (1841).
[76] J. Happel and H. Brenner, *Low Reynolds Number Hydrodynamics* (Martinus Nijhoff, 1983).